A PHYSICAL CONFINEMENT-BASED FORMATION OF SEMICONDUCTOR OXIDE/PLASMONIC NANOPARTICLE HETEROSTRUCTURES

A Thesis

Presented to the Faculty of the Graduate School

of Cornell University

In Partial Fulfillment of the Requirements for the Degree of

Master of Science

in Materials Science and Engineering

Prepared by

Jennifer Eva Tasneem

May 2020

ABSTRACT

Jennifer Eva Tasneem

In nature, biological organisms have substantial control over processes that lead to the formation of biominerals. For example, magnetotactic bacteria utilize the confined volumes of magnetosomes to crystallize magnetic iron oxide particles that are enclosed in lipid bilayer membranes. The organisms are able to form carefully controlled chains of these particles that they use as a compass to navigate the Earth's geomagnetic field. By taking inspiration from such naturally occurring processes, we aim to synthesize functional composites under confinement that possess excellent optoelectronic and photocatalytic properties. Semiconductor oxide and plasmonic metal nanoparticle heterostructures are excellent candidates for studying metal-to-semiconductor energy transfer for optoelectronic applications. Entrapment of plasmonic nanoparticles such as gold and silver within semiconducting materials such as copper oxide and zinc oxide, greatly increases their optical absorption and charge transfer. Two typical morphologies of such heterostructures, such as core-shell nanoparticles and preformed semiconductor oxide structures that are decorated with plasmonic nanoparticles, have been well studied, however, these structures both have limitations on the degree of optical enhancement due to the morphology of the structures. In this study, we used a physical confinement-based technique using track-etched polycarbonate membranes to synthesize heterostructures based on a bio-inspired crystal growth approach to incorporate arrays of plasmonic nanoparticles without the use of insulating surface ligands. By carefully controlling the synthesis

protocol, we are able to tune the spatial distribution of nanoparticles that are entrapped within the semiconductor matrices which can give rise to diverse splitting and broadening of the plasmon peak in the heterostructures. It is important to expand the viable morphologies of heterostructures used in photovoltaic applications because electronic properties depend on the morphology and nanostructure of the composites. Our results demonstrate the flexibility of the physical confinement-based approach to synthesize crystalline architectures which entrap multiple plasmonic nanoparticles within a semiconducting matrix to access a relatively unexplored morphology that can enable promising optoelectronic properties.

BIOGRAPHICAL SKETCH

Jennifer Eva Tasneem was born in June 1993 in Dhaka, Bangladesh to her parents, Mohammad Hasnain Ibne Haleem and Ayesha Akter. From a very young age, she was fascinated with science and mathematics and to incorporate ideas derived from those fields for problem solving and discovery. During high school she developed a keen interest in Chemistry, Physics and Mathematics which led her to pursue an undergraduate degree in Chemistry at Mount Holyoke College in South Hadley, Massachusetts.

At Mount Holyoke, she had the opportunity of combining a liberal arts curriculum with the physical sciences as well as perform academic research in the lab of Dr. Himali Jayathilake. She developed her skills in physical and surface chemistry while synthesizing and characterizing iron oxide nanoparticles for the study of thin films. After her second year, Jennifer traveled to Erlangen, Germany for an internship at the Friedrich Alexander University of Erlangen-Nürnberg (FAU) after securing the Lynk UAF Internship Funding from Mount Holyoke College. At FAU, she was exposed to the world of organic chemistry during her work on synthesizing organic donor molecules for applications in bulk heterojunction solar cells. This internship sparked her interest in materials science and renewable energy. Upon returning to Mount Holyoke, Jennifer immersed in multiple classes in renewable energy, materials science and polymer engineering both at Mount Holyoke College and at the University of Massachusetts, Amherst. These classes solidified her interest to pursue graduate

school in Materials Science and Engineering to further understand the fundamental properties of materials for different applications.

Upon graduation, Jennifer arrived at Cornell University in Ithaca, New York in the department of Materials Science and Engineering. She joined Professor Lara Estroff's lab where she brought her expertise in fundamental chemistry and synthesis to study the formation of functional nanocomposites using a bio-inspired approach. Apart from academic research, Jennifer enjoyed working as a Graduate Peer Adviser at the Cornell Engineering Career Center where she spearheaded drop-in hours for graduate students in the College of Engineering and helped them in navigating a wide variety of career resources and conducted résumé and cover letter critiques as well as practice interviews. After graduation, Jennifer will be joining the School of Chemical Sciences Career Services at the University of Illinois at Urbana-Champaign as a Career Services Coordinator where she will be advising students in Chemistry and Engineering with various aspects of career exploration and professional development.

For Maa and Abbuji, for always believing in me

ACKNOWLEDGMENTS

First and foremost, I would like to thank my advisor and committee chair, Professor Lara Estroff for being an incredible mentor throughout my entire time at Cornell University. Thank you for believing in me and giving me the opportunity of being a part of your research group. Your support and guidance have been an integral part in shaping me to be the scientist I am today. I would also like to thank Professor Jin Suntivich, my second committee member, for his insight and helpful advice on my research.

I am grateful to my undergraduate advisors, Himali Jayathilake and Maria Gomez for being wonderful women in science and for always inspiring me to pursue graduate studies. It may not have been an easy journey, but your support and encouragement along the way has made it worth every bit.

I would like to thank Dr. Abby Goldman for passing me her knowledge about crystal growth and for patiently training me on all the difficult techniques used in my work. I thank Jeffrey Zheng for also being a great resource and for all the help during my training. Additionally, my sincerest appreciation goes out to all the members of the Estroff group for being the best lab mates and an amazing support system.

Last but not the least, I would like to express immense gratitude for the love and support from my family. To my parents: Thank you Maa and Abbuji for supporting me through every step of the way. Thank you for trusting me enough to send me across the world to pursue my passion and dreams as you embraced them as your own. To my sister: Apu, I could not have asked for a better role model to look up to growing up and even today. I would not have been half the person that I am today

without your guidance and encouragement. To my nephew and niece: Rayan and Zara, thank you for coming into my life and brightening up my days. A huge thank you to all my friends and family for their love and prayers, I would not be where I am today without any of it.

TABLE OF CONTENTS

Biographical Sketch...……...…..……iii

Dedication…..…….……v

Acknowledgements…..…….……vi

Table of Contents…..…….……..….viii

List of Figures……..……x

Chapter 1: Introduction and Background……..……..…….1

1.1. Biomineralization as an Inspiration……..……..……..1

1.2. Crystallization in Confinement……..……..…….3

1.3. Incorporation of Secondary Phases into Single Crystalline Matrices……5

1.4. Incorporation of Plasmonic Nanoparticles into Semiconducting Oxides……8

References……..……..…….10

Chapter 2: Using Physical Confinement to Synthesize Semiconductor Oxide/Plasmonic Nanoparticle Heterostructures……...14

2.1 Introduction and Experimental Design ……..……..14

2.1.1 Introduction……..……14

2.1.2 Experimental Design……..……..17

2.2 Experimental…...……..……..…….……18

2.2.1 Materials……..……..……...18

2.2.2 Silver Nanoparticle Synthesis……..…….18

2.2.3 Gold Nanoparticle Synthesis……..……..……19

2.2.4 Loading Nanoparticles into Membrane Pores……...19

2.2.5 Crystallization of Cu_2O/NP Composites in PCTE Membranes…….20

2.2.6 Crystallization of ZnO/NP Composites in PCTE Membranes…….....20

2.2.7 Isolation of Nanorods from Membranes……..……..……..…….21

2.2.8 Scanning Electron Microscopy (SEM) ……..……..…….21

2.2.9 Transmission Electron Microscopy (TEM) ……..……..……..…….21

2.2.10 UV/Vis Spectroscopy…….22

2.3 Results and Discussion……..……..……22

2.3.1 Nanorod Growth……..…….22

2.3.2 Entrapping Gold Nanoparticles in Rods…… …..…….24

2.3.3 Entrapping Silver Nanoparticles in Rods…… …..……...…29

2.3.4 Entrapping Gold-Silver Nanoparticles in Rods…… …..…….....35

2.4 Conclusions……..……..…….38

Appendix 1……..……..……40

References……..……..…….41

Chapter 3: Conclusions and Future Work……..……47

References…..…….51

LIST OF FIGURES

Figure 1.1 Examples from literature of organisms using confinement to control biomineral formation……..…….2

Figure 1.2 Example from literature of SEM images of calcite formation in different sized pores of polycarbonate track-etched membranes……...…….5

Figure 1.3 Example from literature of nanoparticle occlusion into calcite in an agarose gel matrix……..……..7

Figure 2.1 Electron microscope images showing overgrowth of rods off of flat facets and patchy regions showing bulk crystals overgrowing and filling multiple pores……23

Figure 2.2 Schematic to show proposed mechanism of nanorod formation in the pores of polycarbonate track-etched membranes by overgrowth off of adhered crystals…...24

Figure 2.3 UV-Visible absorption spectra of gold nanoparticles before and after loading particles onto a PCTE membrane……...25

Figure 2.4 TEM images of Cu_2O/Au composites with different spatial distribution of nanoparticles due to variation of degas times…….……27

Figure 2.5 TEM images showing ZnO/Au composites with different spatial distribution of nanoparticles due to variation of degas times…….……28

Figure 2.6 UV-Visible absorption spectra of silver nanoparticles before and after loading particles onto a PCTE membrane……..29

Figure 2.7 TEM images of Cu_2O/Ag nanorods obtained from varying the length of degas times……..……..31

Figure 2.8 TEM images of ZnO rods obtained when Ag nanoparticles are loaded onto PCTE membranes with varying degas times ……..……...34

Figure 2.9 UV-Visible absorption spectra of Ag-Au nanoparticles with and without heating to show alloy formation……...……..35

Figure 2.10 TEM images of Cu_2O/Ag-Au nanorods obtained from varying the length of degas times……..……..37

Figure A1 TEM image of citrate stabilized Ag nanoparticles……..…….40

Figure A2 Determining stability of Ag nanoparticles in ammonium hydroxide and zinc nitrate……. ……..40

CHAPTER 1

Introduction and Background

1.1. Biomineralization as an Inspiration

Many marine organisms use biomineralization, the process by which living organisms produce minerals, as a means to synthesize organic/inorganic composites that constitute the structural components of their bodies[1]. These organisms have a high degree of control over the processes that lead to the formation of biominerals, as compared to geologic or synthetic processes that produce similar materials. By studying biomineralization processes, we can learn synthetic approaches that can be tested in the lab to grow a wide range of materials with similar control.

One particularly interesting synthetic tool found in biomineralization is crystallization within confinement[2]. For example, in the unicellular marine algae coccolithophores, the extracellular coccoliths are comprised of uniquely arranged calcite single crystals of specific shape and orientation that are supported on an organic baseplate (Figure 1a & 1b)[3,4]. The precipitation of these crystals occurs within the confines of vesicles inside the cell and the organism is able to control the orientation of crystal nucleation around the baseplate. Limpets, a member of the mollusk family, use nucleation of goethite crystals within chitin fibers during the mineralization of their teeth (Figure 1c)[5]. The oriented inorganic crystals within organic macromolecular matrices provide increased hardness to their teeth and allow them to graze and hold on to rocks during strong tides (Figure 1d)[5]. In another example, magnetotactic bacteria are capable of producing magnetic iron nanocrystals, such as magnetite (Fe_3O_4) or greigite (Fe_3S_4), to

form a chain of particles that allow the microbes to navigate the Earth's geomagnetic field and perform magnetic sensing (Figure 1e)[6]. The crystallization of the particles occurs in confined spaces called magnetosomes, which are membranous intracellular organelles where the particles are enclosed within a lipid bilayer membrane (Figure 1f)[6]. Finally, calcium phosphate can be seen to form within vesicles in neonatal mouse calvaria, which can be used as a model to study human bone mineralization (Figure 1g & 1h)[7]. In all these examples, the organisms use confinement (in vesicles, chitin fibers, magnetosomes, etc.) as a means to control the microscopic morphology, crystallographic orientation, and composition of the resulting biominerals.

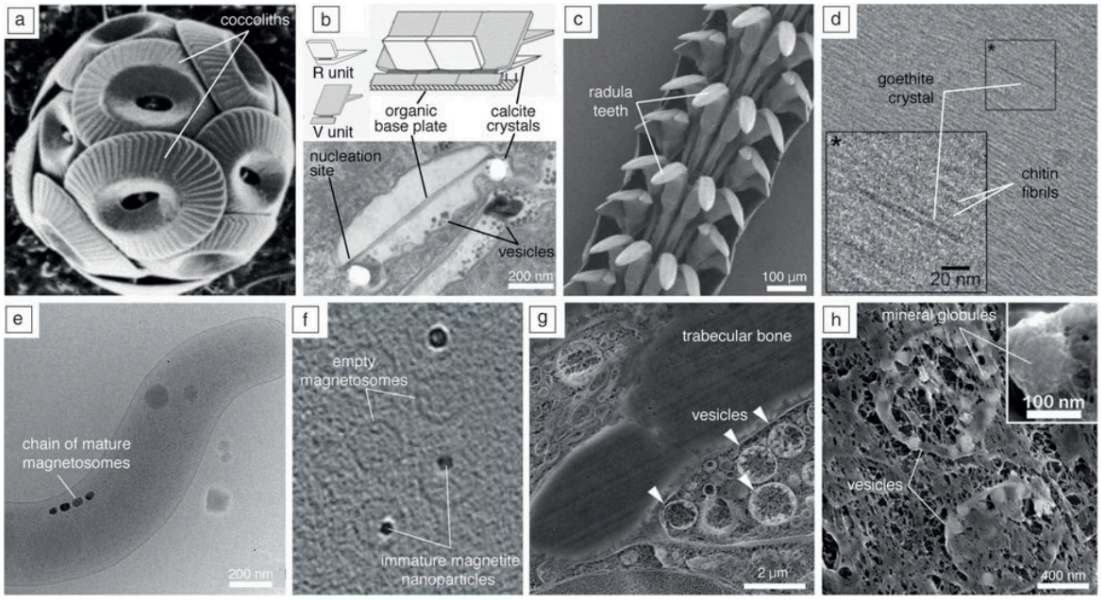

Figure 1.1: Examples of organisms that use confinement as a means to control biomineralization **(a-b)** Coccoliths in coccolithophores are composed of oriented single crystals of calcite which are precipitated in the confines of vesicles inside its unicellular body. The calcite crystals have different shapes and alternating crystallographic orientation and are attached to an organic baseplate. **(c-d)** Limpets have oriented goethite crystals precipitating in chitin fibers, which provide extraordinary hardness to their radula teeth. **(e-f)** Magnetotactic bacteria use the confines of magnetosomes to precipitate iron oxide nanocrystals that are enclosed in lipid bilayer membranes. The microbes form carefully controlled chains of magnetic iron oxide particles to navigate the earth's

magnetic field **(g-h)** In neonatal mouse calvaria, calcium phosphate precipitates can be seen to form in intracellular vesicles. Reproduced with permission from Whittaker, M. L., Dove, P. M. & Joester, D. Nucleation on surfaces and in confinement. *MRS Bull.* **41**, 388–392 (2016). Copyright 2016 Materials Research Society[2].

In addition to unusual formation processes, biominerals often times have improved mechanical, optical, and magnetic properties as compared to their geologic analogues. Thus, the motivating force of this thesis is to develop synthetic processes inspired by these naturally occurring processes and translate them into the work that we do in the laboratory. As such, by using mild synthesis conditions we can aim to achieve a wide range of materials with good functional properties with a high degree of control over crystal morphologies.

1.2. Crystallization in Confinement

As defined by Whittaker et al. crystallization in confinement occurs if the following criteria are met: (i) the crystal phase transformation occurs from a supersaturated solution within a small confined volume (ii) diffusion of one or more of the building blocks of the new crystal phase is hindered[2]. Inspired by biological organisms and processes, research into the use of confinement to form "bio-inspired" materials have been widespread[8]. The complex nature of biological systems makes it difficult to study the processes and factors that influence biomineralization. By using artificial confined systems, new materials and structures can be synthesized according to the shape of the confinements. In addition, confinement allows regulation of the incorporation and spatial distribution of secondary phases in growing crystals[9]. Hence, suitable model systems are crucial in elucidating the mechanism of biomineral formation.

Porous templates such as polycarbonate track-etched membranes (PCTE) can be used to synthesize crystals in confined volumes. Loste et al. used the constrained volumes of the pores of PCTE membranes for the formation calcium carbonate[10]. This study looks at whether confinement can lead to the formation of single crystalline calcite from an amorphous precursor phase. PCTE membranes can be used to template the formation of rod-shaped calcite as opposed to the typical rhombohedral morphology. Membranes of four different pore sizes were used: 10 μm, 3 μm, 0.8 μm and 0.2 μm. At low temperatures of 4-6ºC, the crystallites isolated from the pore in the 10 μm membranes were irregularly shaped and polycrystalline in nature (Figure 1.2a). In contrast, the smaller pore sized membranes had particles that were rod-shaped, had smooth surfaces and were also single crystalline (Figure 1.2b-d). Additionally, calcite crystals growing on the surface of the membranes displayed typical rhombohedral morphology.

When the mechanism of formation of the particles was studied both *in situ* in the membrane and after isolation from the membrane pores over varying incubation periods (between 5 min and 60 min), it could be observed that during the early stages of incubation, spherical particles indicative of amorphous calcium carbonate (ACC) coated the pore walls. When the particles were isolated from the early stages, such as up to 15 min, hollow cylinders were formed with spherical ACC-like particles. On the other hand, longer incubation times led to complete cylinders with faceted ends indicative of crystalline calcite. In the 10 μm membranes, it could be observed that the pores did not completely fill with ACC particles resulting in polycrystalline, irregularly shaped particles even with longer incubation times. In addition, as pore size is decreased, the time required for the formation of crystalline rods also decreased. Hence, by using

constrained volumes, morphological control over the formation of calcite single crystals can be obtained.

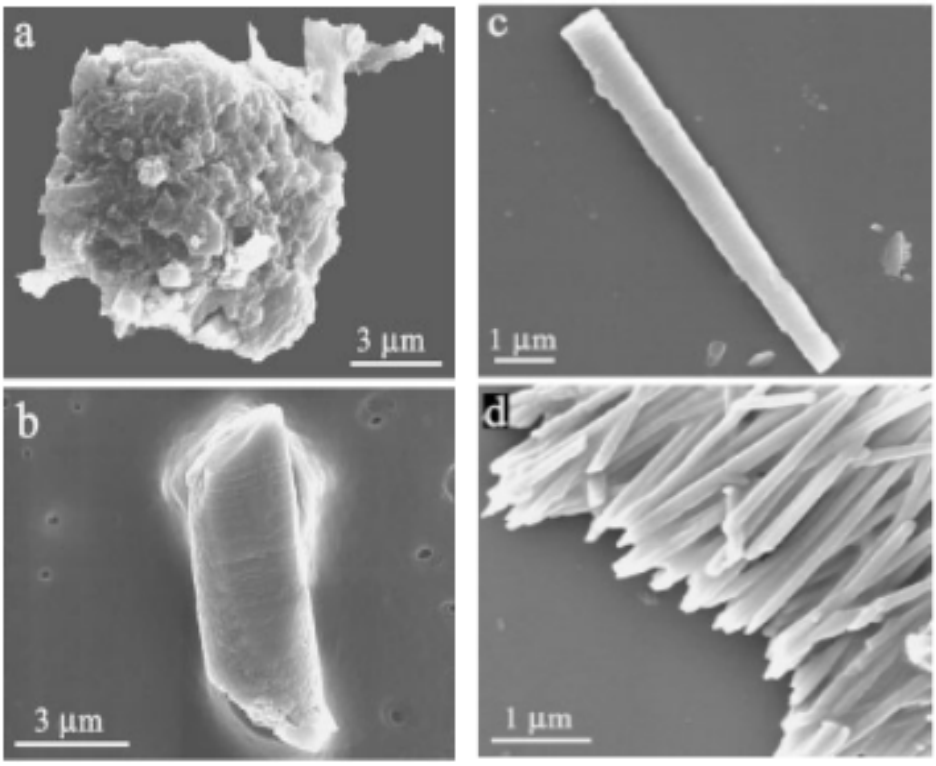

Figure 1.2: Scanning electron micrographs of calcium carbonate particles in different sized pores of polycarbonate track-etched membranes at low temperatures after 24-hour incubation time **(a)** 10 µm **(b)** 3 µm **(c)** 0.8 µm **(d)** 0.2 µm. For the largest pore size **(a)** irregularly shaped morphologies can be isolated from the pores and the crystallites are polycrystalline. For smaller pore sizes, single crystalline calcite rods could be obtained. Reprinted (adapted) with permission from Loste, E., Park, R. J., Warren, J. & Meldrum, F. C. Precipitation of calcium carbonate in confinement. *Adv. Funct. Mater.* **14**, 1211–1220 (2004). Copyright 2004 WILEY-VCH Verlag GmbH & Co. KGaA, Weinheim[10].

1.3. Incorporation of Secondary Phases into Single Crystalline Matrices

Significant research has been conducted on using biomineralization as an inspiration to produce crystalline composite materials with improved functionality[1,11]. However, the factors that come into play for the incorporation of secondary phases into a matrix are

still not well understood. Calcite is an excellent model system to investigate biomineralization strategies[12–14]. For example, self-assembly of latex particles can form 3D colloidal crystals that can be used to template single crystals of calcite[15]. These latex particles can subsequently be removed by tetrahydrofuran (THF) extraction to obtain porous calcite. In this case, surface functionalization of the polymer particles using a carboxylate group played a crucial role in effective ordered embedding of the particles into the crystalline matrix. In fact, studies have shown without surface functionalization of the colloidal crystal template, only irregular calcite crystals can be obtained[16]. Extraction of the secondary phase results in the formation of porous calcite and removal of the particles does not impart any additional functionality to the calcite.

In addition to functionalized nanoparticles, gel matrices have been used as a means to incorporate secondary phases into single crystals. For example, when calcite is grown in a gel matrix, the gel fibers are often incorporated within the crystal without disrupting the single crystallinity[17]. The strength of the gel used plays a role in determining whether the gel becomes incorporated or not[18]. Liu et al. have shown that if the gel strength is high enough, such as in Agarose IB, gel fibers will incorporate within the calcite crystalline matrix[18]. On the other hand, if a weak gel such as agarose IX is used, the growing crystals exclude all foreign phases and grows without the incorporation of gel fibers. By incorporating different types of nanoparticles into gels, additional functionality can be imparted to single crystals grown within gel matrices[19–21]. For example, gels such as agarose loaded with nanoparticles of Au or Fe_3O_4 can used to impart color and paramagnetic properties, respectively, to calcite along with incorporation of gel fibers without significantly disrupting the crystal lattice (Figure 1.3)[20]. Whereas when

nanoparticles were added during solution growth of calcite no such occlusion of particles occurred.

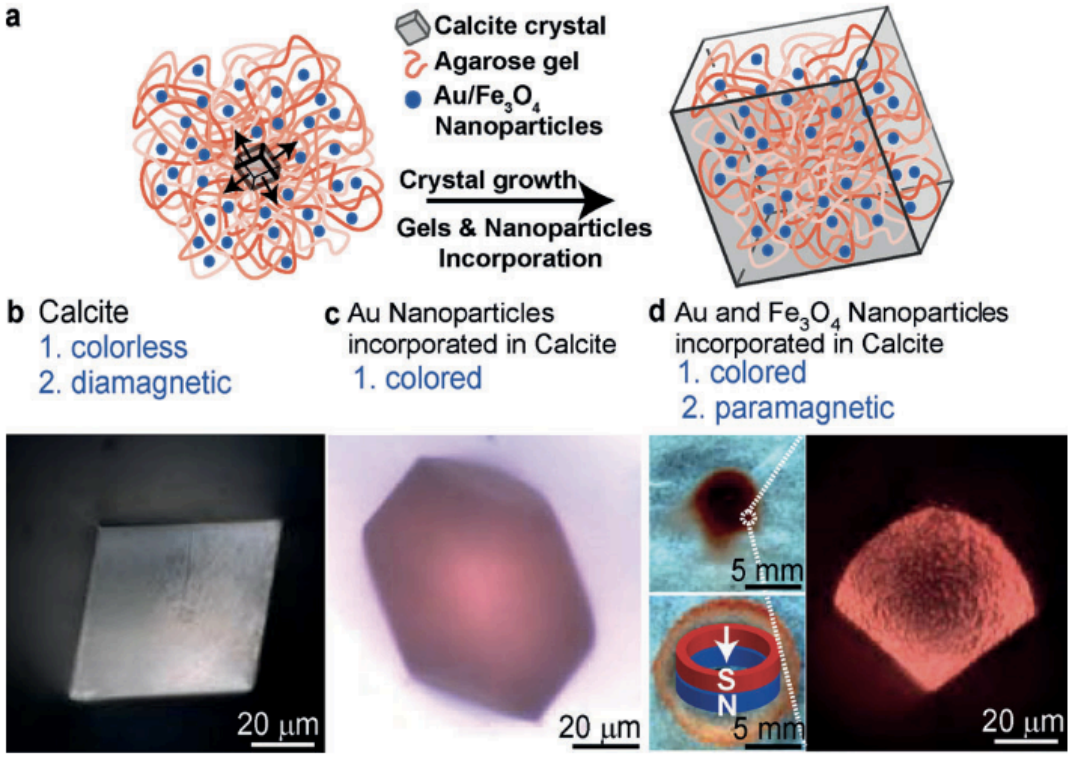

Figure 1.3: (a) Schematic to show the mechanism of nanoparticle loaded gels to form single crystalline calcite with incorporation of nanoparticles and gel fibers. Optical microscopy images of calcite grown in agarose IB gel under different conditions: **(b)** with no nanoparticles, the calcite grown in the gel has a rhombohedral morphology, is colorless and diamagnetic **(c)** when Au nanoparticles are loaded in agarose gel, the calcite grown is colored **(d)** when both Au and Fe_3O_4 nanoparticles are loaded in agarose gel, the calcite grown is colored and is also paramagnetic. Reprinted with permission from Liu, Y., Yuan, W., Shi, Y., Chen, X., Wang, Y., Chen, H., Li, H. Functionalizing Single Crystals: Incorporation of Nanoparticles Inside Gel-Grown Calcite Crystals. *Angew. Chemie - Int. Ed.* **53**, 4127–4131 (2014). Copyright 2014 WILEY-VCH Verlag GmbH & Co. KGaA, Weinheim[20].

While studies with calcite have been very informative, a disadvantage of calcite is that it is not a functional material and is not suitable for diverse applications. Similar

approaches of templating crystalline semiconductor oxide materials using latex particles have been well studied. For example, self-assembled latex particles can be incorporated into single crystals of ZnO and Cu_2O to form three-dimensional ordered macroporous (3DOM) materials[22]. However, adding latex particles into semiconductor oxides also does not lead to additional functionality and the single crystalline 3DOM templates are often used for applications in photonic bandgap crystals and solar cells once the polymer particles are extracted[23]. Hence, the need arises to explore the incorporation of functional secondary phases that can improve the optical properties of semiconductor oxides.

1.4. Incorporation of Plasmonic Nanoparticles into Semiconducting Oxides

In the examples mentioned previously, a confinement based-approach using polycarbonate track-etched membranes can be used to control the morphology of single crystalline calcite to obtain rod-shaped calcite. However, even though calcite is a model biomineral for studying crystallization mechanisms, it is not a functional material for optoelectronic applications. Future work focused on designing crystal matrix/nanoparticle pairs where each of the components have a functional role can address the research gap. Typical morphologies of such heterostructures include core shell nanoparticles and pre-synthesized semiconductor oxide nanostructures with decorated plasmonic metal particles[24–29]. In these heterostructures, both the components play a functional role and are promising materials for studying plasmonic metal-to-semiconductor oxide charge transfer for optoelectronic applications such as photocatalysis and photovoltaics[26,27]. In recent work from our group, arrays of plasmonic nanoparticles such as Au can be completely occluded into crystalline semiconductor oxide of Cu_2O to form

heterostructures by utilizing a physical confinement-based approach using PCTE membranes[30]. This thesis aims to better understand this novel morphology of semiconductor oxide/plasmonic nanoparticle heterostructures by studying the mechanism of formation of the structures as well as diversifying the possible library of material pairs.

References:

1. Nudelman, F. & Sommerdijk, N. A. J. M. Biomineralization as an inspiration for materials. *Angew. Chemie - Int. Ed.* **51**, 6582–6596 (2012).
2. Whittaker, M. L., Dove, P. M. & Joester, D. Nucleation on surfaces and in confinement. *MRS Bull.* **41**, 388–392 (2016).
3. Marsh, M. E., Ridall, A. L., Azadi, P. & Duke, P. J. Galacturonomannan and Golgi-derived membrane linked to growth and shaping of biogenic calcite. *J. Struct. Biol.* **139**, 39–45 (2002).
4. Marsh, M. E. Coccolith crystals of Pleurochrysis carterae: crystallographic faces, organization, and development. *Protoplasma* **207**, 54–66 (1999).
5. Sone, E. D., Weiner, S. & Addadi, L. Biomineralization of limpet teeth: A cryo-TEM study of the organic matrix and the onset of mineral deposition. *J. Struct. Biol.* **158**, 428–444 (2007).
6. Scheffel, A., Gruska, M., Faivre, D., Linaroudis, A., Plitzko, J. M. & Schüler, D. An acidic protein aligns magnetosomes along a filamentous structure in magnetotactic bacteria. *Nature* **440**, 110–114 (2006).
7. Mahamid, J., Sharir, A., Gur, D., Zelzer, E., Addadi, L. & Weiner, S. Bone mineralization proceeds through intracellular calcium phosphate loaded vesicles: A cryo-electron microscopy study. *J. Struct. Biol.* **174**, 527–535 (2011).
8. Jiang, R., Li, B., Fang, C. & Wang, J. Metal/semiconductor hybrid nanostructures for plasmon-enhanced applications. *Adv. Mater.* **26**, 5274–5309 (2014).
9. Ping, H., Xie, H. & Fu, Z. Novel synthesis approaches for new structures in confined space inspired by natural structure-forming processes. *J. Mater.* **3**, 83–95

(2017).

10. Loste, E., Park, R. J., Warren, J. & Meldrum, F. C. Precipitation of calcium carbonate in confinement. *Adv. Funct. Mater.* **14**, 1211–1220 (2004).

11. Weber, E. & Pokroy, B. Intracrystalline inclusions within single crystalline hosts: From biomineralization to bio-inspired crystal growth. *CrystEngComm.* **17**, 5873–5883 (2015).

12. Borukhin, S., Bloch, L., Radlauer, T., Hill, A. H., Fitch, A. N. & Pokroy, B. Screening the incorporation of amino acids into an inorganic crystalline host: The case of calcite. *Adv. Funct. Mater.* **22**, 4216–4224 (2012).

13. Meldrum, F. C. & Hyde, S. T. Morphological influence of magnesium and organic additives on the precipitation of calcite. *J. Cryst. Growth* **231**, 544–558 (2001).

14. Asenath-Smith, E., Li, H., Keene, E. C., Seh, Z. W. & Estroff, L. A. Crystal growth of calcium carbonate in hydrogels as a model of biomineralization. *Adv. Funct. Mater.* **22**, 2891–2914 (2012).

15. Hetherington, N. B. J., Kulak, A. N., Kim, Y., Noel, E. H., Snoswell, D., Butler, M. & Meldrum, F. C. Porous single crystals of calcite from colloidal crystal templates : ACC Is not required for nanoscale templating. *Adv. Funct. Mater.* **27**, 948–954 (2011).

16. Li, C. & Qi, L. Bioinspired fabrication of 3D ordered macroporous single crystals of calcite from a transient amorphous phase. *Angew. Chemie - Int. Ed.* **47**, 2388–2393 (2008).

17. Li, H., Xin, H. L., Muller, D. A. & Estroff, L. A. Visualizing the 3D internal structure of calcite single crystals grown in agarose hydrogels. *Science.* **326**, 1244–

1247 (2009).

18. Li, H. & Estroff, L. A. Calcite growth in hydrogels: Assessing the mechanism of polymer-network incorporation into single crystals. *Adv. Mater.* **21**, 470–473 (2009).

19. Kim, Y. Y., Schenk, A. S., Walsh, D., Kulak, A. N., Cespedes, O. & Meldrum, F. C. Bio-inspired formation of functional calcite/metal oxide nanoparticle composites. *Nanoscale* **6**, 852–859 (2014).

20. Liu, Y., Yuan, W., Shi, Y., Chen, X., Wang, Y., Chen, H. & Li, H. Functionalizing single crystals: incorporation of nanoparticles inside gel-grown calcite crystals. *Angew. Chemie - Int. Ed.* **53**, 4127–4131 (2014).

21. Liu, Y., Zang, H., Wang, L., Fu, W., Yuan, W., Wu, J., Jin, X., Han, J., Wu, C., Wang, Y., Xin, H. L., Chen, H. & Li, H. Nanoparticles incorporated inside single-crystals: enhanced fluorescent properties. *Chem. Mater.* **28**, 7537–7543 (2016).

22. Li, X., Jiang, Y., Shi, Z. & Xu, Z. Two growth modes of metal oxide in the colloidal crystal template leading to the formation of two different macroporous materials. *Chem. Mater.* **19**, 5424–5430 (2007).

23. Li, X., Tao, F., Jiang, Y. & Xu, Z. 3-D ordered macroporous cuprous oxide: fabrication, optical, and photoelectrochemical properties. *J. Colloid Interface Sci.* **308**, 460–465 (2007).

24. Kuo, C., Hua, T. & Huang, M. H. Au nanocrystal-directed growth of Au-Cu2O core-shell heterostructures with precise morphological control. *J. Am. Chem. Soc.* **131**, 17871–17878 (2009).

25. Zhang, L., Blom, D. A. & Wang, H. Au-Cu2O core-shell nanoparticles: A hybrid

metal-semiconductor heteronanostructure with geometrically tunable optical properties. *Chem. Mater.* **23**, 4587–4598 (2011).

26. Kong, L., Chen, W., Ma, D., Yang, Y., Liu, S. & Huang, S. Size control of Au@Cu2O octahedra for excellent photocatalytic performance. *J. Mater. Chem.* **22**, 719–724 (2012).

27. Zheng, Y., Zheng, L., Zhan, Y., Lin, X., Zheng, Q. & Wei, K. Ag/ZnO heterostructure nanocrystals: synthesis, characterization, and photocatalysis. *Inorg. Chem.* **46**, 6980–6986 (2007).

28. Peh, C. K. N., Ke, L. & Ho, G. W. Modification of ZnO nanorods through Au nanoparticles surface coating for dye-sensitized solar cells applications. *Mater. Lett.* **64**, 1372–1375 (2010).

29. Pan, Y., Deng, S., Polavarapu, L., Gao, N., Yuan, P., Sow, C. H. & Xu, Q. Plasmon-enhanced photocatalytic properties of Cu2O nanowire−Au nanoparticle assemblies. *Langmuir* **28**, 12304−12310 (2012).

30. Asenath-Smith, E., Noble, J. M., Hovden, R., Uhl, A. M., DiCorato, A., Kim, Y. Y., Kulak, A. N., Meldrum, F. C., Kourkoutis, L. F. & Estroff, L. A. Physical confinement promoting formation of Cu2O-Au heterostructures with Au nanoparticles entrapped within crystalline Cu2O nanorods. *Chem. Mater.* **29**, 555–563 (2017).

CHAPTER 2

Using Physical Confinement to Synthesize Semiconductor Oxide/Plasmonic Nanoparticle Heterostructures*

* Co-contributors of this chapter include Dr. Abby R. Goldman who performed the Cu_2O/Au composite growth and Jeffrey X. Zheng who performed the ZnO/Au growths

2.1 Introduction and Experimental Design

2.1.1 Introduction

Semiconductors such as cuprite (Cu_2O) and zinc oxide (ZnO) are promising materials for many optoelectronic applications such as in photovoltaic devices and photocatalysis[1]. Not only are cuprite and zinc oxide attractive materials due to their wide variety of applications, they are also favorable due to their earth abundance, low cost and multitude of synthesis pathways[2–4]. One of the challenges for using them in optoelectronic applications, however, is that the optical absorption of these materials in the visible light spectrum is low. This property results in inefficient conversion of light to energy. Much research has been conducted to find ways to increase the optical absorption of semiconducting oxides by using plasmonic nanoparticles of noble metals such as gold (Au), silver (Ag), and platinum (Pt)[5]. Plasmonic nanoparticles possess a unique property called Localized Surface Plasmon Resonance (LSPR)[6]. LSPR enhances electromagnetic fields after the absorption of light, which is confined in a small area around an isolated nanostructure. Hence incorporating plasmonic nanoparticles within a nanostructured semiconducting oxide can enhance the carrier density and overall optical absorption of the heterostructure due to the LSPR effect[7–9].

There are several well-known morphologies of semiconductor/plasmonic nanoparticle heterostructures that have been studied in the past[5]. Among these, core-shell nanostructures that have a plasmonic metal core and a semiconductor oxide shell have gained considerable attention due to the synergistic optoelectronic properties of the two components. For example, core-shell heterostructures with an Au core and Cu_2O shell have been widely studied with good control over their overall morphologies[10–12]. The main limitation of these structures is that a majority of them are only able to encapsulate single plasmonic particles. Even though both the components are in intimate contact with each other, having a single nanoparticle per structure, limits the plasmon enhancement. Besides core-shell structures, semiconductor nanostructures decorated with plasmonic metals have also been widely studied[13–17]. There are several ways to prepare such heterostructures. For example, molecular linkers such as long chain organic ligands can be used to attach pre-synthesized plasmonic nanoparticles onto the surface of pre-synthesized semiconductor nanostructures using mechanical agitation[18,19]. Even though this process is simple, as it allows for both the components to be prepared separately to make a wide variety of heterostructures, this method poses the problem of less efficient plasmon enhancement due to the presence of an insulating barrier at the interface[20]. In another approach, secondary phases such as functionalized nanoparticles are trapped within single crystal matrices grown from aqueous solutions[21]. For example, magnetite nanoparticles functionalized by a diblock copolymer can be trapped within a single crystalline ZnO host in a simple, one-pot synthesis[22].

The degree of incorporation and arrangement of plasmonic nanoparticles within the semiconductor plays a major role on the final optoelectronic properties of the

heterostructure[1,5,23]. In addition to the these variables, one of the major challenges that dictate the performance of semiconductor/plasmonic nanoparticle heterostructures is the presence of long chain organic ligands that act as surfactants and stabilize plasmonic nanoparticle assemblies[24,25]. Organic ligands that act as spacers between nanoparticles prevent aggregation of those particles but are also electrically insulating, resulting in less direct contact at the semiconductor and metal interface. In photocatalytic applications, presence of long chain organic ligands and polymer molecules can result in significant losses in catalytic activity as these molecules can block active sites by obstructing access of reagents and also strongly interact with the metal surfaces. Hence, new semiconductor/plasmonic metal heterostructures that are free of organic ligands and in which multiple plasmonic metal nanoparticles can be integrated can open up new possibilities for enhanced optoelectronic properties.

As described in Chapter 1, crystal growth in confinement is one approach to achieving the incorporation of secondary phases such as plasmonic nanoparticles into semiconducting oxides such as ZnO and Cu_2O. To understand how confinement can promote incorporation, consider the role of crystallization pressure, the force a growing crystal exerts on its surroundings, in repelling foreign particles during unrestricted solution growth[26]. In order to counterbalance the repulsive crystallization pressure, physical confinement can be used to immobilize secondary phases and force incorporation of the particles by the growing crystals. For example, previous work in our group demonstrated a method of growing Cu_2O nanorods in polycarbonate track-etched (PCTE) membranes to entrap Au nanoparticles within a semiconducting oxide matrix of Cu_2O[27]. In that method, vapor diffusion of a reducing agent, hydrazine, is used to

crystallize Cu_2O from an aqueous solution in the membrane pores that are previously loaded with Au. Using this technique, Au nanoparticle assemblies can be incorporated within Cu_2O without disrupting the crystallinity of the semiconducting oxide as can be observed by the presence of continuous lattice fringes at the metal-semiconductor interface.

2.1.2 Experimental Design

In the current work, we expand the library of composite materials that can be grown using the PCTE membrane method. In this work, we use both cuprite and zinc oxide as the semiconductor "host" material, and Au, Ag, and Ag-Au nanoparticles as the plasmonic "guests". Cu_2O is a p-type semiconductor and has a direct band gap of approximately 2.17 eV making it a suitable material for applications in solar cells[28,29], photocatalysis[30] and as electrode materials in batteries[31]. On the other hand, ZnO is an n-type semiconductor with a direct, wide band gap of 3.37 eV[32]. ZnO also has a variety of applications in photovoltaics such as dye-sensitized solar cells (DSSCs)[33], battery electrodes[34] and gas sensors[35].

We first study the growth of Cu_2O rods with entrapped Au nanoparticles (Cu_2O/Au) by vapor diffusion to dive deeper into the formation mechanism of the nanostructures. Depending on the precise synthesis protocol and using a degas step, the spatial arrangement of the entrapped nanoparticles can be tuned. We then use this strategy to grow ZnO/Au nanorods within the pores of PCTE membranes. Finally, we report the diversity of this approach to incorporate Ag nanoparticles to form Cu_2O/Ag and also Cu_2O/Ag-Au heterostructures. Depending on the solution chemistry and the compatibility of the materials used to form the composites, this method presents a

versatile physical confinement-based approach to form functional semiconductor/plasmonic nanoparticle heterostructures.

2.2 Experimental

2.2.1 Materials

All materials were used as received without further purification. Copper (II) sulfate pentahydrate (98%, Sigma-Aldrich), sodium citrate tribasic dihydrate (>98%, Sigma-Aldrich), sodium hydroxide pellets (99.2%, Fisher), hydrazine hydrate (78-82%, Sigma-Aldrich), zinc nitrate hexahydrate (98%, Sigma-Aldrich), ammonium hydroxide solution (28-30%, VWR), dichloromethane (DCM, 99.8%, Sigma-Aldrich), ethanol (100%, Pharmco-Aaper), gold (III) chloride trihydrate (99.99%, Aldrich), silver nitrate (99.9%, Alfa Aesar), tannic acid (Sigma-Aldrich), polycarbonate track-etched membranes (Whatman Nuclepore™, 25 mm membrane diameter, 0.05 μm pore size). Water passed through a Millipore system (ρ = 18.2 MΩ) was used in all experiments.

2.2.2 Silver Nanoparticle Synthesis

Citrate stabilized silver nanoparticles were synthesized using a method adapted from Bastús et al[36]. Briefly, a three-necked flask containing 79 mL of deionized water and 17.5 mL of 5 mM trisodium citrate (SC) solution was brought to a boil while stirring vigorously under reflux. After boiling had commenced, 1 mL of 2.5 mM tannic acid was added to the flask and the solution was heated further for 15 min. Subsequently, 1 mL of 25 mM $AgNO_3$ was added to the solution. The solution immediately changed color to bright yellow, after which the solution was quenched on ice for 30 min. The resultant Ag NPs were used without any further purification.

2.2.3 Gold Nanoparticle Synthesis

Citrate-stabilized gold nanoparticles were synthesized using the Turkevich method[37]. Briefly, 50 mL of a 3.55×10^{-4} M $HAuCl_4$ solution was brought to a boil while stirring under reflux. After boiling commenced, 1.5 mL of 1 w/v% trisodium citrate solution was added to the solution. The solution color progressed from colorless to grey to purple to deep red within 5 min. The solution was refluxed for an additional 30 min. After cooling in air for 30 min, the particles were dialyzed (MWCO = 3.5K) against deionized water balanced to pH 10 using 1 M NaOH with three exchanges over the course of 72 h.

2.2.4 Loading Nanoparticles into Membrane Pores

A vacuum filtration process was used to load the nanoparticles into the pores of the PCTE membranes using a previously published method from our group[27]. Briefly, aliquots (0.4 mL x 25) of 10 mL nanoparticle solution are pulled through the membrane pores by vacuum filtration. The membrane was then flipped over, and filtration was repeated with the same solution. It was ensured that the membrane did not completely dry during the loading process to prevent any solid metal deposits. The particle-loaded membranes were stored in the nanoparticle solution until use in crystallization (< 3 days). Following loading, the membrane is degassed in 10 mL of the ionic crystal growth solution (copper sulfate solution for Cu_2O and zinc nitrate solution for ZnO) for the desired amount of time (ranging from no degas to 24 hr degas) prior to nanorod growth.

For Ag-Au loading: For Ag and Au loading, 5 mL of Ag nanoparticle solution was filtered through the PCTE membranes using the above method first, followed by loading

5 mL of Au nanoparticle solution using the same method. The degassing of membranes was carried out immediately after Ag-Au loading without storage overnight.

2.2.5 Crystallization of Cu_2O/NP Composites in PCTE Membranes

Crystallization of Cu_2O is carried out by vapor diffusion of hydrazine hydrate into a modified Fehling's solution as previously established[27]. The nanoparticle loaded membrane is degassed under vacuum in a glass vial containing copper sulfate solution (10 mL, 0.068 M) for preferred amount of time (ranging from no degas to 24 hr degas) prior to Cu_2O growth. In a new glass vial, a copper complex was made by mixing 2 mL each of copper sulfate hexahydrate (0.068 M), trisodium citrate (0.074 M) and sodium hydroxide solution (0.12 M). The particle-loaded membrane is added to the basic copper citrate solution after degassing. Hydrazine was added to a petri dish (3.5 mL of 80.2% hydrazine hydrate with 16.5 mL water) and subsequently, the vial containing the loaded membrane is balanced on a half glass slide over the petri dish inside the double-walled reaction chamber. The reaction is carried out with the internal temperature of the reactor at 64°C for 8 hours after which the membrane turns red and the solution turns from bright blue to pale grey.

2.2.6 Crystallization of ZnO/NP Composites in PCTE Membranes

Nanoparticle loaded membranes are degassed under vacuum in zinc nitrate solution (10 mL) for preferred amount of time (ranging from no degas to 24 hr degas) prior to ZnO growth. In a glass vial, 10 mL of 50 mM zinc nitrate solution is added followed by loaded membrane after degassing. Using a similar method as the Cu_2O growth, ZnO is crystallized in the membranes pores by using vapor diffusion of 20 mL of

0.72 wt% ammonium hydroxide and the reaction is carried out at 60°C for 24 hours after which white precipitates are observed on the membrane and the solution is clear.

2.2.7 Isolation of Nanorods from Membranes

After crystallization using vapor diffusion, membranes were removed from growth solution and rinsed with DI-H_2O (3 times) and ethanol (2 times) until the solution runs clear. This washing is followed by gentle scraping of the membrane with weigh paper to remove bulk crystals on the membrane surface. Finally, the membranes were air dried for 10 min. The nanorods are isolated from the membranes by dissolving the polycarbonate in dichloromethane. The products were centrifuged (11,000 g, 5 min), rinsed in dichloromethane (3 times) and ethanol (2 times), and redispersed. Microscopy samples were prepared by drop casting these solutions directly on Formvar coated and/or lacey carbon transmission electron microscope (TEM) copper grids.

2.2.8 Scanning Electron Microscopy (SEM)

Scanning electron microscopy was performed using a Mira3 LM field emission scanning electron microscopy (SEM) at 10 keV. To prevent charge buildup, samples are carbon coated prior to imaging. Imaging is done using both secondary electrons (SE) and backscattered electrons (BSE) and analyzed using ImageJ. Brighter regions in BSE images are indicative of higher Z materials.

2.2.9 Transmission Electron Microscopy (TEM)

Bright-field transmission electron microscopy is performed using a FEI T12 Spirit TEM operating at 120 kV and images are analyzed using ImageJ.

2.2.10 UV/Vis Spectroscopy

Optical absorption spectra of the nanoparticle solutions were measured from 300-700 nm using a Cary 5000 UV-Vis-NIR Spectrophotometer.

2.3 Results and Discussion

2.3.1 Nanorod Growth

Before looking at the growth of the composites, we first observe the growth of the semiconducting oxides in the membranes. Firstly, empty PCTE membranes without any nanoparticles are placed in cuprite and ZnO growth solutions separately to crystallize Cu_2O and ZnO. To get a better understanding of the how the nanorod growth occurs, we dissolved the membrane before scraping the surface adhered crystals. TEM and SEM images of these samples show faceted crystals of Cu_2O and ZnO with multiple rods growing off of one side (Figure 2.1a & 2.1b). If instead, the membrane is left intact after growth and scraped to remove surface adhered crystals, we can observe the growth patterns of the nanorods in the membrane. Backscattered electron images reveal patches of bright spots on the membrane where crystals of ZnO had covered the surfaces (Figure 2.1c, d).

Based upon these observations of 1) faceted crystals with attached nanorods (Fig. 2.1a, b) and 2) patches of nanorods grown within the membranes (Fig. 2.1c, d), we propose that nanorods form in the membrane pores by overgrowth off of surface adhered crystals (Figure 2.2). During the vapor diffusion process, crystals of the semiconductor oxide form in solution. These crystals have roughly micron-sized edges and also have flat facets. After crystallizing in the solution, the flat facets fall on the surface of the membrane and continuation of the crystal growth results in the formation of the nanorods

in the pores. Each bulk crystal covers a sizeable area of the membrane surface at once and hence causes a large number of pores to be filled by overgrowth (Figure 2.1c).

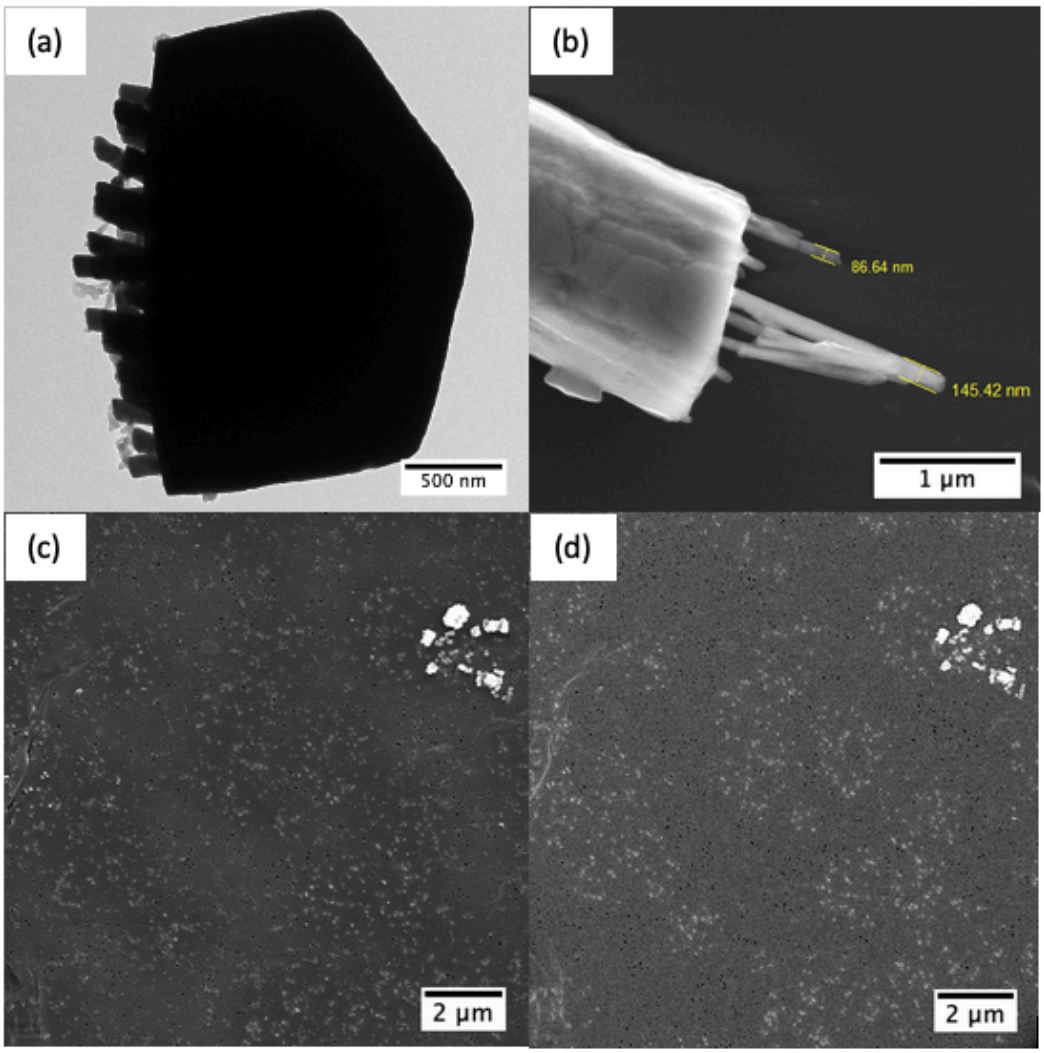

Figure 2.1. (a) TEM image of a single crystal of Cu_2O showing multiple rods that overgrow off of the flat facet **(b)** SEM image of a single crystal of ZnO showing multiple rods still attached **(c)** Secondary electron SEM image of ZnO grown in a membrane after scraping to remove surface adhered crystals **(d)** Corresponding backscattered electron image shows patches of bright regions indicating higher Z materials than the carbonate membrane. The patches appear due to surface adhered crystals overgrowing and filling multiple pores.

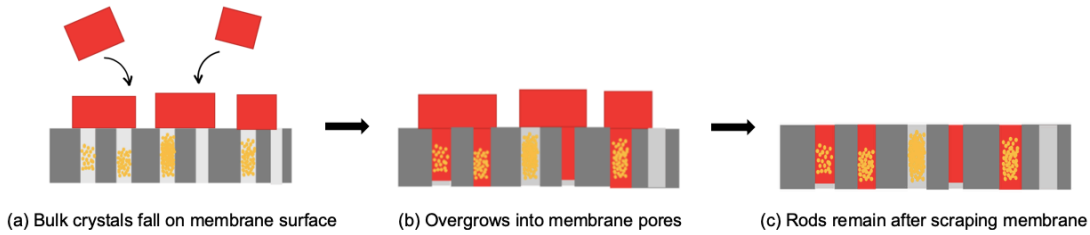

Figure 2.2. Proposed mechanism for membrane templated nanorod growth shown schematically via cross section of a track-etched membrane. **(a) C**rystals grow in solution and fall onto the membrane surface and cover pores that are loaded with nanoparticles. Not all the pores get loaded with nanoparticles **(b)** Growth continues off of surface adhered crystals and fills the membrane pores forming cylindrical rods. **(c)** Scraping the membrane surface gently removes the larger crystals, leaving nanorods in the membrane pores, which can be isolated by dissolving the membrane.

Based upon this proposed mechanism by which nanorods form, we can say that materials that form large, faceted bulk crystals under ambient conditions can be used to expand the library of possible semiconductor matrices. PCTE membranes are inexpensive, commercially available and a good technique to template the growth of semiconductor/plasmonic metal heterostructures. However, it has to be ensured that the synthesis conditions required for the growth are somewhat mild as the membrane pores get distorted at temperatures above 110°C and the membranes dissolve at high solution pH. Vapor diffusion synthesis of both Cu_2O and ZnO fulfill these criteria.

2.3.2 Entrapping Gold Nanoparticles in Rods

We next aim to immobilize Au nanoparticles in the membrane pores and form composite nanorods. This was achieved by mechanically filtering the plasmonic nanoparticle solution through PCTE membranes prior to vapor diffusion growth of the semiconductor oxides. Absorption spectrum obtained for the citrate-stabilized Au

nanoparticles show the characteristic plasmon resonance peak for gold at 525 nm (Figure 2.3). When the spectrum of the effluent is obtained after loading a membrane with particles by vacuum filtration, the intensity of the peak is seen to decrease due to decrease in nanoparticle concentration suggesting effective loading of nanoparticles into membrane pores.

We think that nanoparticles get trapped within the membrane pores due to numerous particles attempting to flow through pores at the same time. As a result, they clog the pores and form plugs of particles. It is very challenging to determine the factors that come into play in the immobilization of nanoparticles through small channels. In depth studies into filtration suggest that particles can assemble in channels or pores when certain ratios of particle size to pore size are met[38]. In the case of our synthesized Au nanoparticles, the nanoparticles have a diameter of roughly 16±1 nm and the pore sizes are ~50 nm. However, other factors such as concentration of the solution, flow rate and ionic strength of the solution may also have interesting effects on pore filling which we have yet to explore.

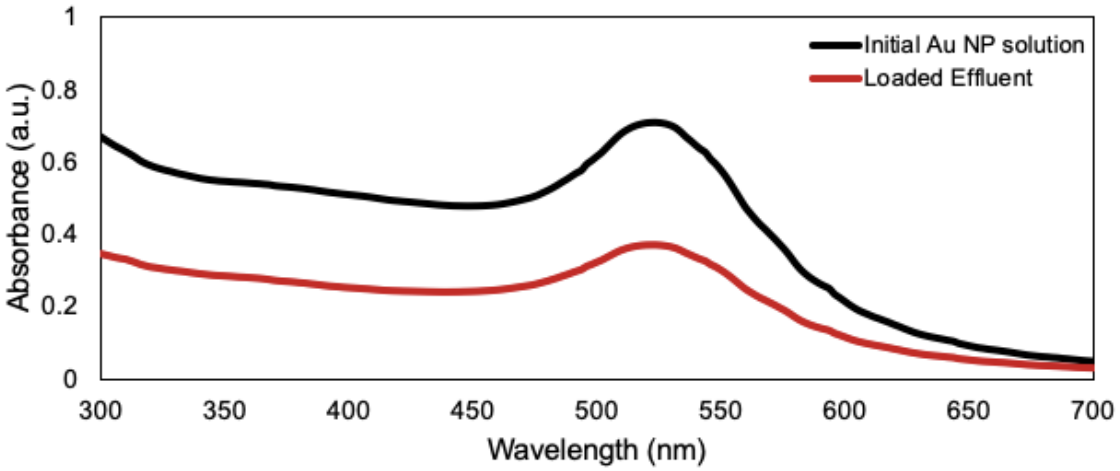

Figure 2.3: Absorption spectrum of Au NPs reveals its characteristic plasmon resonance peak at 525 nm (black). Decrease in intensity of the characteristic plasmon peak suggests that nanoparticles were loaded onto membrane (red).

By introducing a degas step prior to the growth of Cu_2O or ZnO we are able to tune the spatial distribution of the nanoparticles over the length of the rod. For this step, a PCTE membrane that is loaded with nanoparticles is placed in the respective ionic solution, copper sulfate solution for Cu_2O and zinc nitrate solution for ZnO, and then degassed under vacuum for the preferred amount of time (between 0 to 24 hours). When PCTE membranes loaded with Au nanoparticles undergo vapor diffusion to grow Cu_2O we can see that Cu_2O/Au composite rods form where the nanoparticles are found as "plugs" that span only part of the total length of the rod in the central region if the membrane is degassed for one hour (Figure 2.4a). Some empty rods are also seen since not all pores are clogged with nanoparticles. When degassing for greater than 12 hr, the nanoparticles are seen to be dispersed and spread along the majority of the length of the rod (Figure 2.4b). We hypothesize that upon loading, Au nanoparticles are first entrapped in a plug-like structure and upon prolonged degas in an ionic solution, the nanoparticle array gets reorganized and forms a more dispersed configuration. During the degas step, we propose two ways by which the nanoparticles rearrange: (1) repulsive electrostatic forces due to the presence of ions pushes nanoparticles away from each other, and (2) as ionic solution is pulled through the pores of the membrane, removal of air bubbles in the pores mechanically disrupts the nanoparticle array and causes rearrangement. To investigate the effect of degassing further, future experiments in ionic solutions ranging from low to high ionic strengths as well as degassing in de-ionized water can be performed to confirm if the ionic strength of the solution during degas is a factor in tuning nanoparticle arrangement.

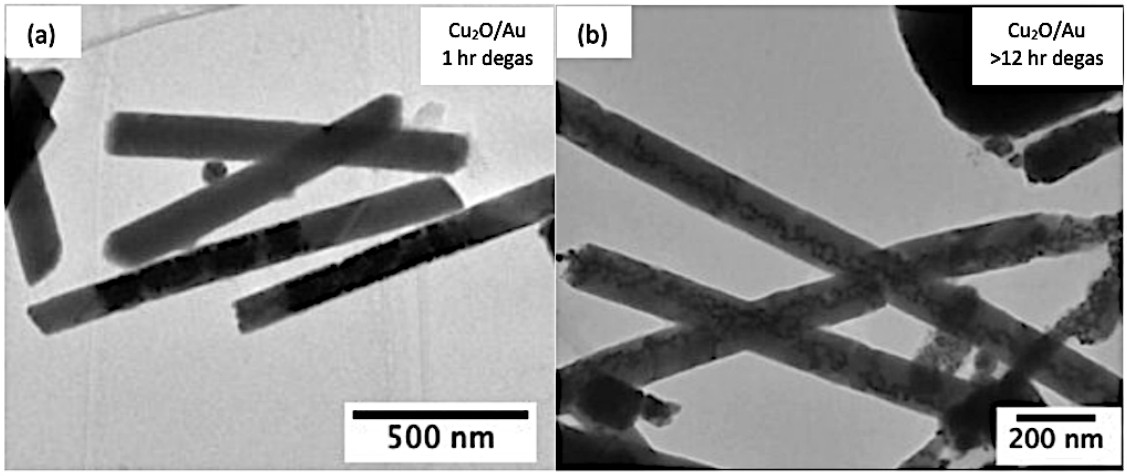

Figure 2.4: (a) TEM of Cu_2O/Au NP composite rods grown where the nanoparticles are found as "plugs" that span part of the total length of the rod after 1 hr degas. **(b)** TEM of Cu_2O/Au NP composite rods where the nanoparticles are dispersed along majority of the length of the rod after degassing for >12 hr.

In case of ZnO rods, we can see that eliminating the degas step prior to vapor diffusion leads to the formation of "plugs" of just nanoparticles (Figure 2.5a). Along with plugs of nanoparticles, some empty rods are also observed. It may be that the nanoparticle array is somehow fused or glued together by the ionic growth solution but the mechanism by which these plugs stay intact is not fully understood. When introducing a short, 1 hr degas prior to ZnO growth, complete disruption of the isolated plugs of nanoparticles occurs and instead, "clusters" of nanoparticles are observed in and around ZnO rods (Figure 2.5b). Furthermore, when degassed for greater than 12 hr, nanoparticles are similarly dispersed along the length of the rod as for Cu_2O/Au (Figure 2.5c). We hypothesize that rods in which the nanoparticles are well-dispersed along the length of semiconductor matrix will provide enhanced LSPR effect as there is more surface area of the nanoparticles in contact with the semiconductor to allow greater charge transfer.

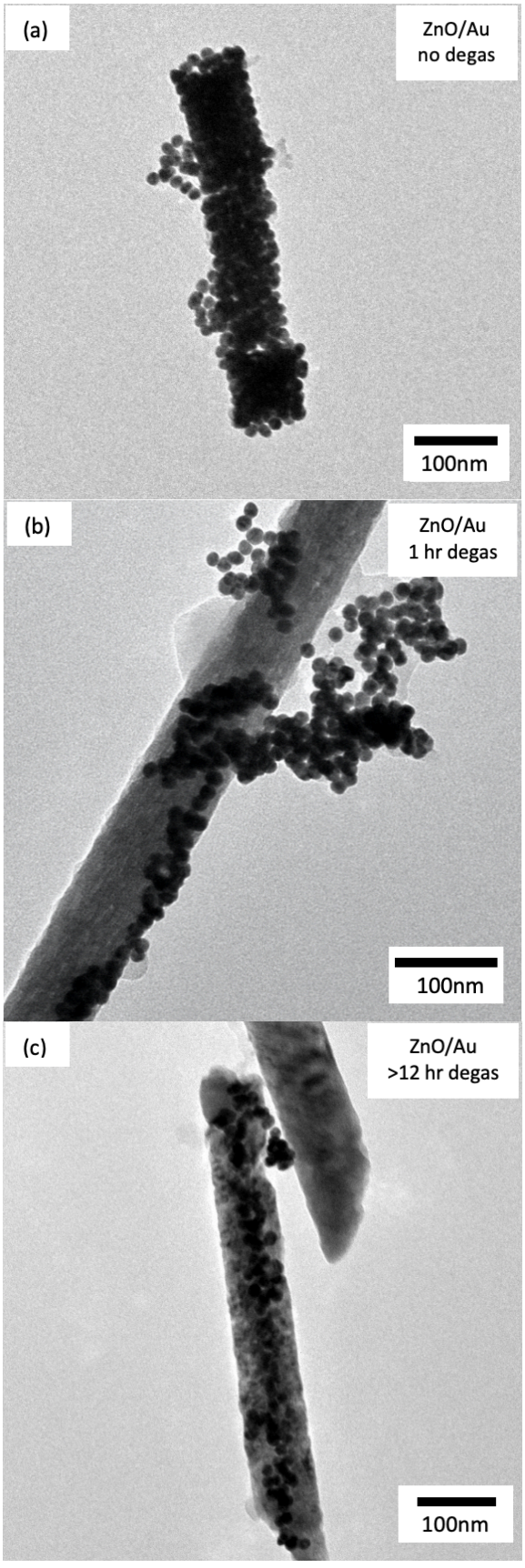
(a)
ZnO/Au
no degas
100nm
(b)
ZnO/Au
1 hr degas
100nm
(c)
ZnO/Au
>12 hr degas
100nm

Figure 2.5: Representative images of ZnO/Au nanorods obtained from varying the length of degas times: **(a)** no degas forms many isolated "plugs" of nanoparticles as well as empty rods (not shown) **(b)** short, 1 hr degas forms "clusters" of nanoparticles around ZnO rods **(c)** prolonged, >12 hr degas causes dispersed nanoparticles in rods. We can see that the spatial distribution of nanoparticles within the rods changes as a function of the degas time.

2.3.3 Entrapping Silver Nanoparticles in Rods

With more insight about the mechanism by which nanorods grow in pores and with the ability to tune the spatial distribution of nanoparticles in the membrane pores, we next aim to incorporate silver nanoparticles into Cu_2O and ZnO rods. The silver nanoparticle synthesis was adapted from a method by Bastús et al[36]. The synthesized nanoparticles have a diameter of roughly 24±7nm as analyzed by ImageJ (Figure A1). Similar to Au nanoparticle loading, when Ag nanoparticles are loaded onto PCTE membranes the intensity of the characteristic plasmon resonance peak for silver at 400 nm (Figure 2.6) is seen to decrease, suggesting effective loading of nanoparticles into membrane pores.

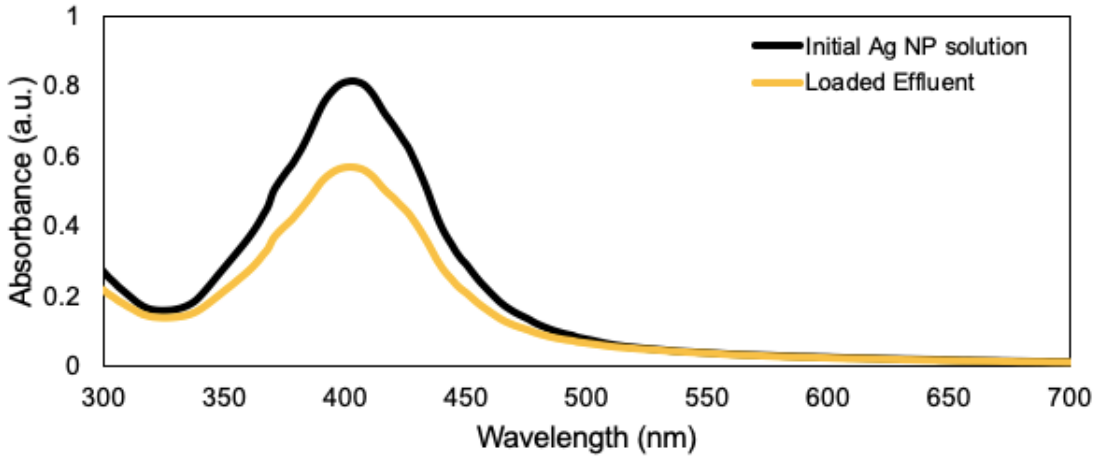

Figure 2.6: Absorption spectrum of Ag NPs reveals its characteristic plasmon resonance peak at 400nm (black). Decrease in intensity of the characteristic plasmon peak suggests that nanoparticles were loaded onto membrane (yellow).

When Ag nanoparticles are incorporated to form Cu_2O/Ag composites, it is observed that foregoing the degas step causes nanoparticles to be entrapped across majority of the length of the rod as well as across the entire diameter of the rod. On the other hand, it is also observed that these rods have a large number of surface defects or "notches" (Figure 2.7a). During the loading process, since the nanoparticles are clogged across the entire diameter of the pores, poor overgrowth of the bulk crystals into the pores results in more surface defects. Due to the defects, the rods are more susceptible to fracture at the defect sites and as a result on average, shorter rods are observed. Increasing the degas times to greater than 12 hours results in higher aspect ratio rods. When the membrane is degassed for 18 hours prior to growth, the nanoparticles are found across the entire length and diameter of the rod, and in this case fewer surface defects are observed (Figure 2.7b). Finally, with 24 hour degas, the particles are seen to arrange in long chains in the central region of the rods (Figure 2.7c). The surface of the rods appears to be smoother with fewer defects due to better overgrowth of bulk crystals into the pores. In this case as well, prolonged degas causes rearrangement of the nanoparticles trapped in the membrane pores.

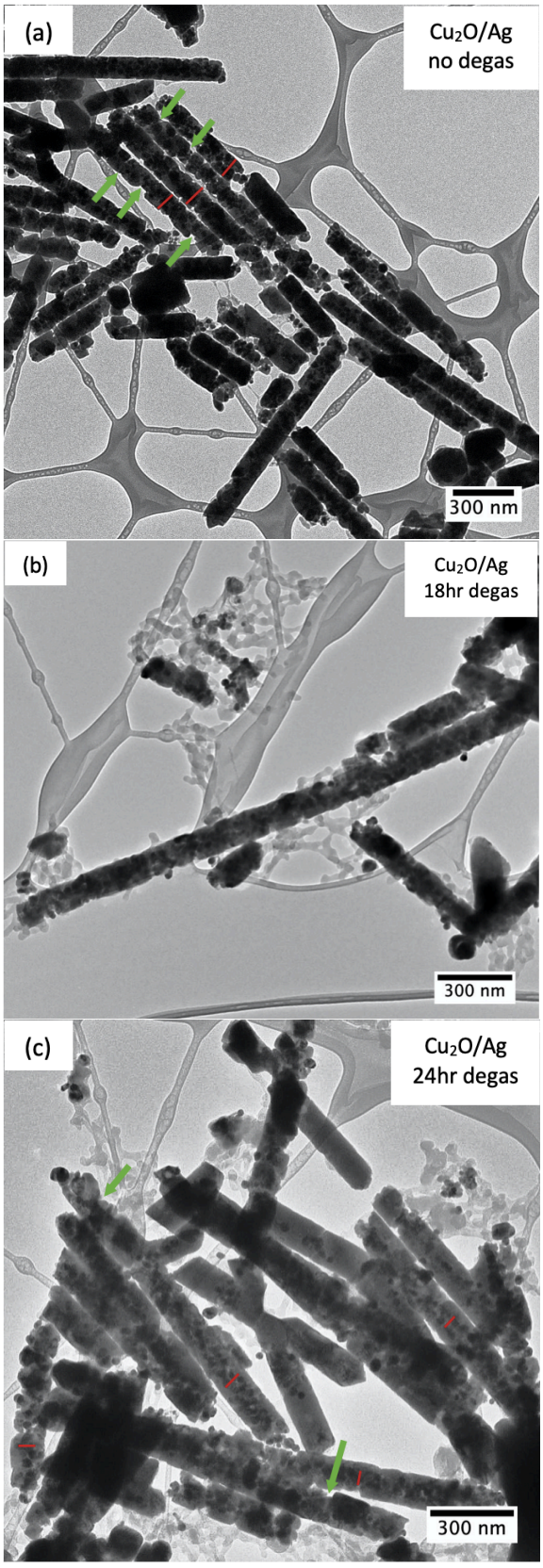
(a)
Cu2O/Ag
no degas
300 nm
(b)
Cu2O/Ag
18hr degas
300 nm
(c)
Cu2O/Ag
24hr degas
300 nm

Figure 2.7: Representative TEM images of Cu_2O/Ag nanorods obtained from varying the length of degas times: **(a)** no degas forms rods where nanoparticles are found along the majority of the length and also the diameter of the rods (indicated by longer red lines). These rods have a large number of "notches", or surface defects (indicated by green arrows) **(b)** 18 hr degas forms rods of higher aspect ratios and nanoparticles are found along the majority of the length and also the diameter of the rods **(c)** prolonged, 24hr degas causes nanoparticles to be dispersed in chains along the central region in rods (indicated by shorter red lines). There are also fewer surface defects in this case.

When Ag nanoparticles are immobilized in the pores of PCTE membranes to form ZnO/Ag composites, no nanoparticles can be observed in the TEM images even with varying degas times. Foregoing the degas step in this case produces short, flaky rods (Figure 2.8a). When the membrane is degassed for 18 hours, longer rods are produced without any nanoparticles (Figure 2.8b). Finally, with 24 hour degas even though no nanoparticles were occluded in the matrix, the ZnO rods formed on average had the highest aspect ratio (Figure 2.8c). Hence, stability tests for Ag nanoparticles were conducted to see the effect of the reagents on the particles. It was observed that when Ag nanoparticles were added to ammonium hydroxide solution, the bright yellow color of the particles disappear within a few hours indicating that they dissolve in the basic solution (Figure A2a). During the degas step, zinc nitrate solution is pulled through the membrane pores under vacuum for the desired amount of time. When looking at the stability of Ag nanoparticles in zinc nitrate, the particles are seen to crash out in the solution as observed by the brown precipitates (Figure A2b). Both the base and salt used in this reaction are not compatible with Ag nanoparticles. Therefore, in order to diversify the possible pairs of semiconductor oxide and plasmonic nanoparticles, it is important to first confirm the compatibility of the materials used to preserve the viability of the final heterostructure. Longer degas times mean that the pores are exposed to more ions in the growth solution

for longer time periods. Thus, greater diffusion of ions in the pores produces a modified ionic environment which supports the formation of higher aspect ratio rods.

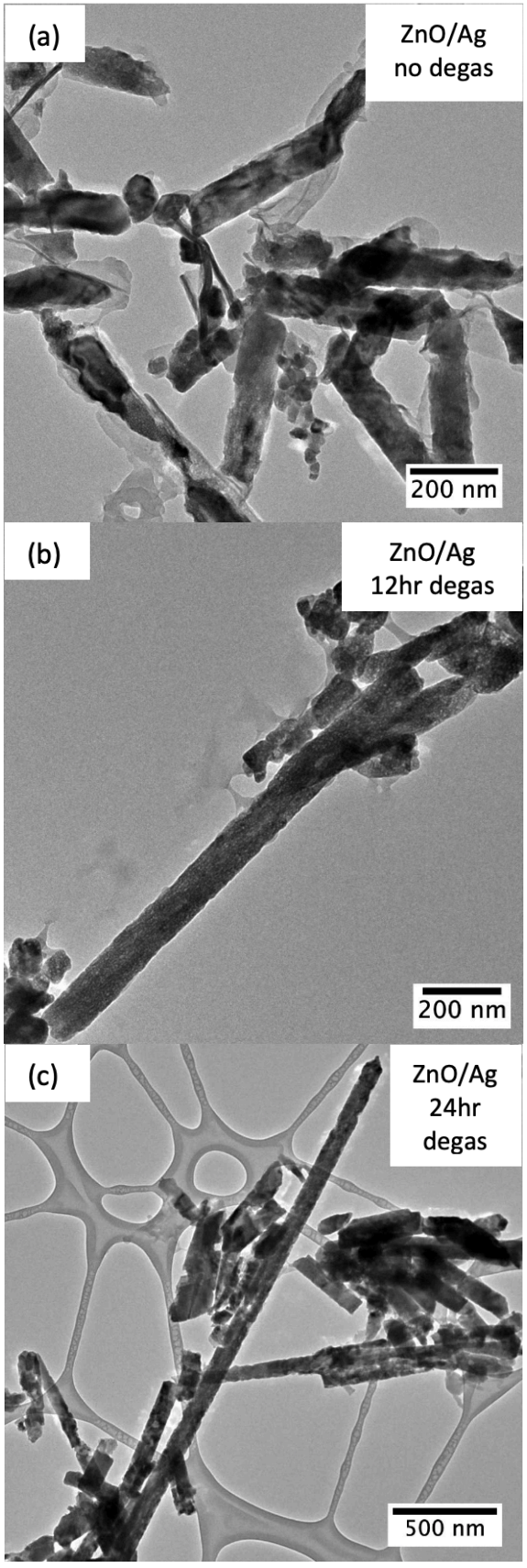
(a)
ZnO/Ag
no degas
200 nm
(b)
ZnO/Ag
12hr degas
200 nm
(c)
ZnO/Ag
24hr
degas
500 nm

Figure 2.8: Representative TEM images of rods obtained from growth of ZnO when Ag nanoparticles are used with increasing of degas times. Silver nanoparticles are not suitable for use with the ZnO system hence no nanoparticles can be seen in the rods **(a)** no degas produces short, flaky rods **(b)** 18 hr degas forms rods of higher aspect ratio **(c)** prolonged, 24 hr degas produces rods with highest aspect ratios.

2.3.4 Entrapping Gold-Silver Nanoparticles in Rods

Gold and silver nanoparticles are excellent plasmonic particles in particular because of their localized surface plasmon resonance (LSPR), which in turn greatly enhances the sensitivity of Raman scattering. Using a mixed gold and silver nanoparticle system, a considerably stronger surface enhanced Raman scattering (SERS) can be observed as opposed to the monometallic counterparts[39]. This can allow enhanced properties for photocatalytic applications and increase the efficiency of photoelectric conversion in solar cells by expanding the wavelength region for SERS.

When equal volumes of gold and silver nanoparticles are mixed without heating and without the presence of the reducing agent hydrazine, two separate plasmon peaks for Au (~530 nm) and Ag (~410 nm) can be observed (Fig. 2.9). However, when this mixture is heated in the presence of hydrazine, a single peak within the intermediate region at 496 nm is observed, which indicates the formation of Au-Ag alloy[40,41]. Au-Ag nanoparticles are well known for their catalytic activities[42,43].

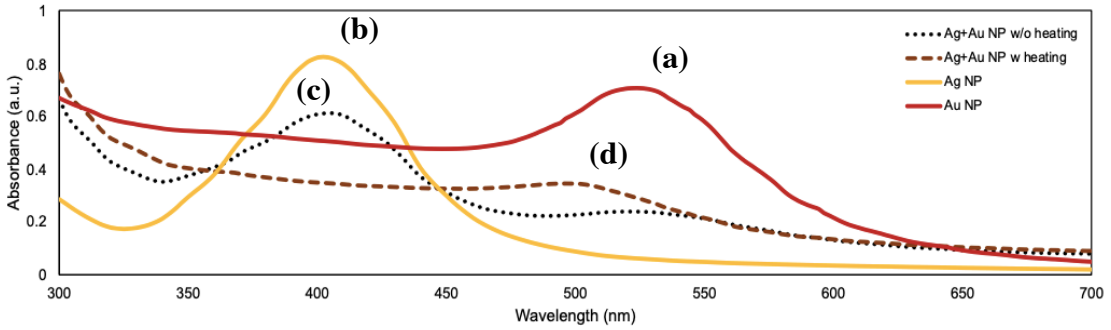

Figure 2.9. (a) Absorption spectrum of Au NPs reveals its characteristic plasmon resonance peak at 525 nm. **(b)** Absorption spectrum of Ag NPs reveals its characteristic

plasmon resonance peak at 400 nm. The broadness of the peaks indicates some polydispersity. **(c)** Absorption spectrum of a solution of equal volumes of Ag and Au nanoparticles reveals the two separate plasmon peaks for Ag and Au. **(d)** When this solution is exposed to heat and hydrazine, a single peak is observed at 496 nm indicating the presence of an Ag-Au alloy.

To observe the effects of a mixed Ag and Au nanoparticle system, Ag and Au nanoparticles are loaded sequentially onto PCTE membranes. First, 5 mL of Ag nanoparticle solution was loaded onto a membrane followed by 5 mL of Au nanoparticle solution. After the sequential loading of the nanoparticles, the membrane is degassed for preferred amount of time (ranging from no degas to 24 hr degas). The loaded and degassed membranes are then placed in the Cu_2O growth solution to allow the formation of Cu_2O/Ag-Au composites. Similar to the single nanoparticle system of Cu_2O/Ag, foregoing the degas step in the case of Cu_2O/Ag-Au forms rods with many surface defects where nanoparticles are packed along the entire length and diameter of the rods (Figure 2.10a). Increasing degas time to greater than 12 hours results in the nanoparticles being more dispersed along the length of the rods while decreasing the number of surface defects (Figure 2.10b). Finally, degassing for 24 hours results in high aspect ratio rods due to the diffusion of more ions adjacent to the pore surfaces (Figure 2.10c). Hence, degassing the membrane prior to vapor diffusion allows us to carefully control the spatial arrangement of nanoparticles trapped in the membrane pores. Future experiments on measurement of optoelectronic properties can allow us to gain better understanding about how the spatial arrangement plays a role in affecting the properties. We hypothesize that by using a mixed system such as Au-Ag, we will be able to access enhanced LSPR effects for optoelectronic applications.

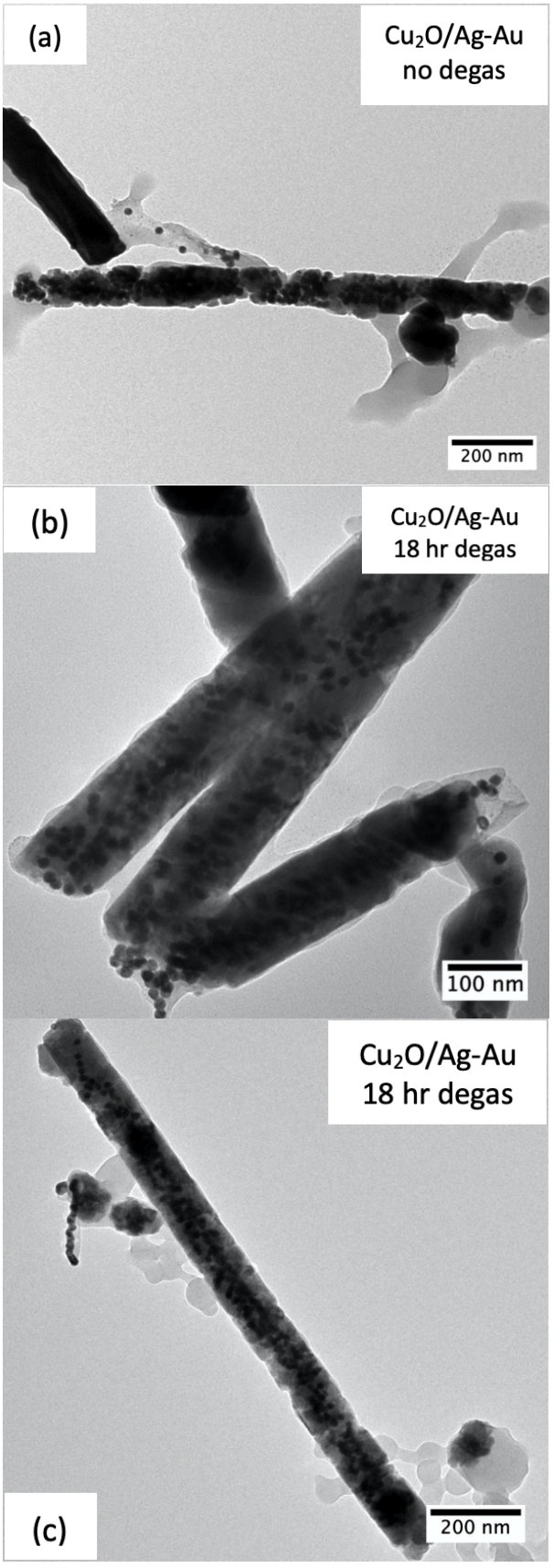
(a)
Cu2O/Ag-Au
no degas
200 nm
(b)
Cu2O/Ag-Au
18 hr degas
100 nm
Cu2O/Ag-Au
18 hr degas
(c)
200 nm

Figure 2.10: Representative images of Cu_2O/Ag-Au nanorods obtained from varying the length of degas times: **(a)** no degas forms rods where nanoparticles are found along the majority of the length and also the diameter of the rods. These rods have a large number of "notches", or surface defects **(b)** 18 hr degas forms shorter rods with nanoparticles dispersed along the majority of the length with fewer notches **(c)** prolonged, 24hr degas forms high aspect ratio nanorods with nanoparticles dispersed in chains along the central region in rods. There are also fewer surface defects in this case.

2.4 Conclusions

We demonstrate a versatile method for the growth of nanorods with occluded nanoparticle arrays using a physical confinement-based approach using polycarbonate track-etched membranes. By studying the growth of Cu_2O and ZnO in the membranes we learn that nanorods form within membrane pores by overgrowth off of crystals that grow in solution. We showed successful occlusion of Au nanoparticles without the use of long chain, insulating ligands to form Cu_2O/Au and ZnO/Au composites. Furthermore, we are able to tune the spatial distribution of nanoparticles within the nanorods by allowing the nanoparticle loaded membrane to degas in an electrolyte solution. We hypothesize that by changing the distribution of the nanoparticles within the semiconductor matrix, a finer control over the optoelectronic properties of these heterostructure composites can be achieved. Finally, we further expanded the repertoire of possible structures by entrapping Ag nanoparticles in Cu_2O to form Cu_2O/Ag and also a mixture of Ag and Au NPs in Cu_2O to form Cu_2O/Ag-Au heterostructures. ZnO/Ag nanoparticles are not viable because silver nanoparticles are not stable in the growth solutions used for ZnO crystallization. Further work should focus on property measurements of these unexplored heterostructure geometries and determine how tuning spatial arrangement of the plasmonic metals can modify both the optical absorption as well as the metal-to-semiconductor energy transfer of the composites. The ability to create dispersed

plasmonic nanoparticle arrays without the use of molecular linkers is promising for further improvements to the optoelectronic properties due to increased absorption[44].

APPENDIX 1

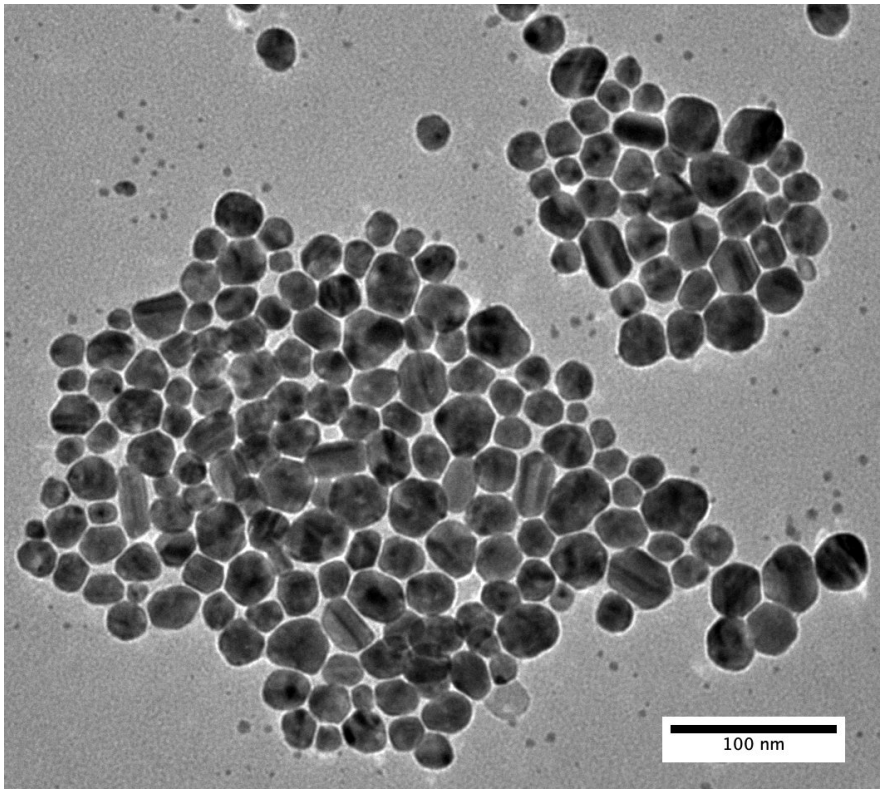

Figure A1: Citrate stabilized silver nanoparticles were prepared by a method adapted from Bastús et al[36] (diameter roughly 24±7nm).

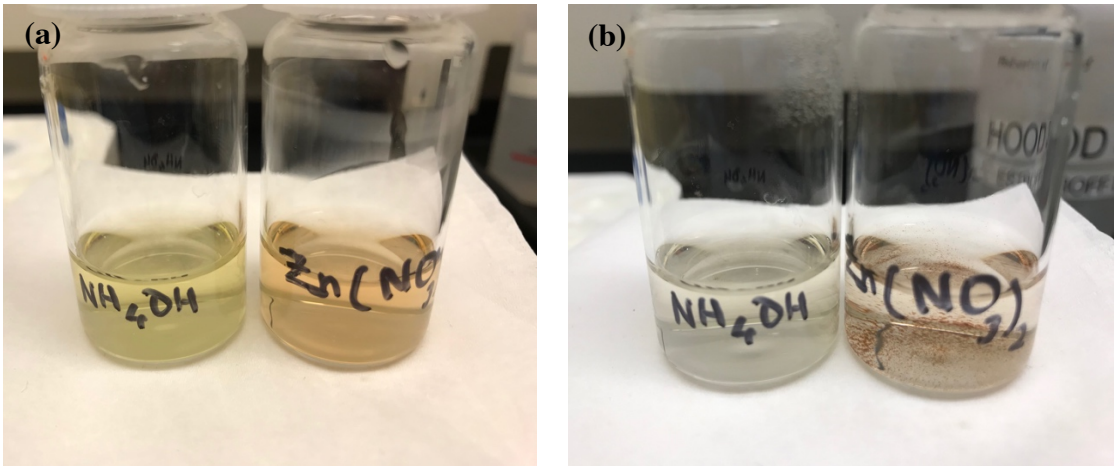

Figure A2: (a) Immediately after silver nanoparticles (bright yellow) are added to ammonium hydroxide and zinc nitrate solutions **(b)** After ~3 hours, the pale-yellow color of silver nanoparticles turns colorless indicating that the nanoparticles dissolve in ammonium hydroxide. Additionally, the nanoparticles are seen to crash out in zinc nitrate solution.

References:

1. Ma, L., Chen, S., Shao, Y., Chen, Y., Liu, M., Li, H., Mao, Y. & Ding, S. Recent progress in constructing plasmonic metal/semiconductor hetero-nanostructures for improved photocatalysis. *Catalysts* **8**, 634 (2018).
2. Ghijsen, J., Tjeng, L. H., Elp, J. van, Eskes, H., Westerink, J. & Sawatzky, G. A. Electronic structure of Cu2O and CuO. *Am. Phys. Soc.* **38**, 322–330 (1988).
3. Kegel, J., Povey, I. M. & Pemble, M. E. Zinc oxide for solar water splitting: A brief review of the material's challenges and associated opportunities. *Nano Energy* **54**, 409–428 (2018).
4. Wang, Z. L. Nanostructures of zinc oxide. *Mater. Today* **7**, 26–33 (2004).
5. Jiang, R., Li, B., Fang, C. & Wang, J. Metal/semiconductor hybrid nanostructures for plasmon-enhanced applications. *Adv. Mater.* **26**, 5274–5309 (2014).
6. Willets, K. A. & Van Duyne, R. P. Localized surface plasmon resonance spectroscopy and sensing. *Annu. Rev. Phys. Chem.* **58**, 267–297 (2007).
7. Atwater, H. A. & Polman, A. Plasmonics for improved photovoltaic devices. *Nat. Mater.* **9**, 205–214 (2010).
8. Cushing, S. K. & Wu, N. Plasmon-enhanced solar energy harvesting. *Electrochem. Soc. Interface* **2 (c)**, 63–67 (2013).
9. Cushing, S. K. & Wu, N. Progress and perspectives of plasmon-enhanced solar energy conversion. *J. Phys. Chem. Lett.* **7**, 666–675 (2016).
10. Kuo, C., Hua, T. & Huang, M. H. Au nanocrystal-directed growth of Au-Cu2O core-shell heterostructures with precise morphological control. *J. Am. Chem. Soc.* **131**, 17871–17878 (2009).

11. Zhang, L., Blom, D. A. & Wang, H. Au-Cu2O core-shell nanoparticles: A hybrid metal-semiconductor heteronanostructure with geometrically tunable optical properties. *Chem. Mater.* **23**, 4587–4598 (2011).

12. Kong, L., Chen, W., Ma, D., Yang, Y., Liu, S. & Huang, S. Size control of Au@Cu2O octahedra for excellent photocatalytic performance. *J. Mater. Chem.* **22**, 719–724 (2012).

13. Cozzoli, P. D., Comparelli, R., Fanizza, E., Curri, M. L., Agostiano, A. & Laub, D. Photocatalytic synthesis of silver nanoparticles stabilized by TiO2 nanorods: a semiconductor/metal nanocomposite in homogeneous nonpolar solution. *J. Am. Chem. Soc.* **126**, 3868–3879 (2004).

14. Zheng, Y., Zheng, L., Zhan, Y., Lin, X., Zheng, Q. & Wei, K. Ag/ZnO heterostructure nanocrystals: synthesis, characterization, and photocatalysis. *Inorg. Chem.* **46**, 6980–6986 (2007).

15. Peh, C. K. N., Ke, L. & Ho, G. W. Modification of ZnO nanorods through Au nanoparticles surface coating for dye-sensitized solar cells applications. *Mater. Lett.* **64**, 1372–1375 (2010).

16. Zhu, H., Zhu, E. & Ou, G. Fe3O4–Au and Fe2O3–Au hybrid nanorods: layer-by-layer assembly synthesis and their magnetic and optical properties. *Nanoscale Res. Lett.* **5**, 1755–1761 (2010).

17. Pan, Y., Deng, S., Polavarapu, L., Gao, N., Yuan, P., Sow, C. H. & Xu, Q. Plasmon-enhanced photocatalytic properties of Cu2O nanowire–Au nanoparticle assemblies. *Langmuir* **28**, 12304–12310 (2012).

18. Xiao, F., Wang, F., And, X. F. & Zheng, Y. A green and facile self-assembly

preparation of gold nanoparticles/ZnO nanocomposite for photocatalytic and photoelectrochemical applications. *J. Mater. Chem.* **22**, 2868–2877 (2012).

19. Yu, H., Ming, H., Zhang, H., Li, H., Pan, K., Liu, Y., Wang, F., Gong, J. & Kang, Z. Au/ZnO nanocomposites: Facile fabrication and enhanced photocatalytic activity for degradation of benzene. *Mater. Chem. Phys.* **137**, 113–117 (2012).
20. Jana, N. R., Wang, Z. L. & Pal, T. Redox catalytic properties of palladium nanoparticles: surfactant and electron donor-acceptor effects. *Langmuir* **16**, 2457–2463 (2000).
21. Ning, Y., Fielding, L. A., Nutter, J., Kulak, A. N., Meldrum, F. C. & Armes, S. P. Spatially controlled occlusion of polymer-stabilized gold nanoparticles within ZnO. *Angew. Chemie - Int. Ed.* **58**, 4302–4307 (2019).
22. Kulak, A. N., Grimes, R., Kim, Y. Y., Semsarilar, M., Anduix-Canto, C., Cespedes, O., Armes, S. P. & Meldrum, F. C. Polymer-directed assembly of single crystal zinc oxide/magnetite nanocomposites under atmospheric and hydrothermal conditions. *Chem. Mater.* **28**, 7528–7536 (2016).
23. Kochuveedu, S. T., Jang, Y. H. & Kim, D. H. A study on the mechanism for the interaction of light with noble metal-metal oxide semiconductor nanostructures for various photophysical applications. *Chem Soc Rev* **42**, 8467–8493 (2013).
24. Baumgardner, W. J., Whitham, K. & Hanrath, T. Confined-but-connected quantum solids via controlled ligand displacement. *Nano Lett.* **13**, 3225–3231 (2013).
25. Kovalenko, M. V., Scheele, M. & Talapin, D. V. Colloidal nanocrystals with molecular metal chalcogenide surface ligands. *Science.* **324**, 1417–1421 (2009).
26. Khaimov-Mal'kov, V. Y. *Growth of Crystals Vol. 2. Growth of Crystals*

(Shubnikov, A. V., Sheftal, N. N., 1959).

27. Asenath-Smith, E., Noble, J. M., Hovden, R., Uhl, A. M., DiCorato, A., Kim, Y. Y., Kulak, A. N., Meldrum, F. C., Kourkoutis, L. F. & Estroff, L. A. Physical confinement promoting formation of Cu2O-Au heterostructures with Au nanoparticles entrapped within crystalline Cu2O nanorods. *Chem. Mater.* **29**, 555–563 (2017).

28. Musa, A. O., Akomolafe, T. & Carter, M. J. Production of cuprous oxide, a solar cell material, by thermal oxidation and a study of its physical and electrical properties. *Sol. Energy Mater. Sol. Cells* **51**, 305–316 (1998).

29. Ait, A., Atourki, L., Abouabassi, K., Elfanaoui, A., Bouabid, K., Ihlal, A., Benmokhtar, S. & Ouafi, M. Growth and characterization of Cu2O for solar cells applications. *AIP Conf. Proc.* **2056**, 020006 (2018).

30. Zhang, Y., Jiu, B., Gong, F., Chen, J. & Zhang, H. Morphology-controllable Cu2O supercrystals: Facile synthesis, facet etching mechanism and comparative photocatalytic H2 production. *J. Alloys Compd.* **729**, 563–570 (2017).

31. Chen, K., Song, S. & Xue, D. Faceted Cu2O structures with enhanced Li-ion battery anode performances. *CrystEngComm.* **17**, 2110–2117 (2015).

32. Klingshirn, C. The luminescence of ZnO under high one- and two-quantum excitation. *Phys. Stat. Sol.* **71**, 547–556 (1975).

33. Baxter, J. B. & Aydil, E. S. Nanowire-based dye-sensitized solar cells. *Appl. Phys. Lett.* **86**, 053114 (2005).

34. Zhang, W., Du, L., Chen, Z., Hong, J. & Yue, L. ZnO nanocrystals as anode electrodes for lithium-ion batteries. **2016**, 10–12 (2016).

35. Xu, J., Pan, Q. & Tian, Z. Grain size control and gas sensing properties of ZnO gas sensor. *Sensors Actuators B* **66**, 277–279 (2000).

36. Bastús, N., Merkoçi, F., Piella, J. & Puntes, V. Synthesis of highly monodisperse citrate-stabilized silver nanoparticles of up to 200 nm: Kinetic control and catalytic properties. *Chem. Mater.* **26**, 2836–2846 (2014).

37. Turkevich, J. & Stevenson, P. C. A study of the nucleation and growth processes in the synthesis of colloidal gold. *Discuss. Faraday Soc.* **11**, 55–75 (1951).

38. Xia, Y., Yin, Y., Lu, Y. & McLellan, J. Template-assisted self-assembly of spherical colloids into complex and controllable structures. *Adv. Funct. Mater.* **13**, 907–918 (2003).

39. Akiyama, T. Facile fabrication and raman scattering enhancement properties of mixed gold and silver nanoparticle layers. *e-Journal Surf. Sci. Nanotechnol.* **10**, 157–160 (2012).

40. Liu, S., Chen, G., Prasad, P. N. & Swihart, M. T. Synthesis of monodisperse Au, Ag, and Au-Ag alloy nanoparticles with tunable size and surface plasmon resonance frequency. *Chem. Mater.* **23**, 4098–4101 (2011).

41. Mallin, M. P. & Murphy, C. J. Solution-phase synthesis of Sub-10 nm Au-Ag alloy nanoparticles. *Nano Lett.* **2**, 1235–1237 (2002).

42. Wang, C., Yin, H., Dai, S. & Sun, S. A general approach to noble metal-metal oxide dumbbell nanoparticles and their catalytic application for CO oxidation. *Chem. Mater.* **22**, 3277–3282 (2010).

43. Liu, J. H., Wang, A. Q., Chi, Y. S., Lin, H. P. & Mou, C. Y. Synergistic effect in an Au-Ag alloy nanocatalyst: CO oxidation. *J. Phys. Chem. B* **109**, 40–43 (2005).

44. Hanske, C., Tebbe, M., Kuttner, C., Bieber, V., Tsukruk, V. V., Chanana, M., König, T. A. F. & Fery, A. Strongly coupled plasmonic modes on macroscopic areas via template-assisted colloidal self-assembly. *Nano Lett*. **14**, 6863–6871 (2014).

CHAPTER 3

Conclusion and Future Work

This thesis aimed to demonstrate the versatility of a physical confinement-based approach to synthesize semiconductor/plasmonic nanoparticle composites. By mimicking naturally occurring processes that are easily accessible to bio-organisms, this work aims to use biomineralization as an inspiration and translate it into the work that we do in the laboratory to produce functional materials with enhanced properties. We use polycarbonate track-etched membranes to entrap nanoparticles in the physical confines of the pore channels. Prior to this thesis, this method was applied to achieve nanorods of Cu_2O with plasmonic Au nanoparticles entrapped in the semiconductor matrix[1]. In order to prove that this method can be used to grow other materials, we applied our knowledge and understanding of the crystal growth mechanism to also grow ZnO rods with Au nanoparticles trapped within them. By using a crucial degas step in the synthesis process, we are able to tune the spatial distribution of the nanoparticles along the length of the rods. By using shorter degas times we find that Au nanoparticles are in the form of "plugs" or "clusters" that are localized in and around the nanorods. On the other hand, increasing the degas time to greater than 12 hours leads to the rearrangement of nanoparticles in the form of chains along the length of the rod.

With more knowledge about nanorod formation in membrane pores and a better grasp on tuning the spatial distribution of nanoparticles, I next used Ag nanoparticles to form new semiconductor/plasmonic nanoparticle pairs. Solution chemistry plays a critical role in determining which materials and heterostructures can be achieved using this synthetic approach. I was able to successfully incorporate Ag nanoparticles within Cu_2O

to form Cu_2O/Ag structures and also tune the spatial arrangement of nanoparticles within the rods by varying degas times. On the other hand, ZnO/Ag composites could not be synthesized because the Ag nanoparticles were not stable in the growth solutions required. Hence, in order to successfully diversify the repertoire of possible structures, it is first necessary to determine the compatibility of the materials used for synthesis. Furthermore, by using an Ag-Au alloy I was also able to synthesize Cu_2O/Ag-Au heterostructures and tune the nanoparticle dispersity within the matrix. While further work is needed to determine the optoelectronic properties of these heterostructures, Ag-Au alloy particles have previously been researched because of their enhanced catalytic effect[2,3]. Aside from tuning the spatial arrangement of nanoparticles within the rods by using varying degas times, longer degas times can also be used to obtain higher aspect ratio rods. By degassing for longer periods of times, the local ionic environment in and around pores is modified due to the diffusion of ions which supports the formation of longer rods.

Although by degassing nanoparticle loaded membranes, we are able to control the nanoparticle spatial dispersity in the pores, more information about what aids nanoparticle trapping in the pores as well as the factors that affect spatial dispersity can give us a better control of the degas step. We need to consider the concentration of the nanoparticle solution, flow rate during vacuum filtration of nanoparticles, as well as the ionic strength of the salt solution in which the membrane is degassed. I think that the presence of ions in the salt solution exerts electrostatic forces, which aid the dispersion of the nanoparticles during prolonged degas. Hence, by degassing membranes in de-ionized water, as well as salt solutions of increasing ionic strength, we could confirm if ionic

strength is a factor during degas to gain more insight on the electrostatic forces that come into play during this crucial step.

Thus far, we have only considered confinement of nanospheres in our approach of producing functional nanocomposites. This choice was mainly due to the ease of synthesis and our group's expertise with nanospheres. However, expanding this approach even further to incorporate other shapes of nanoparticles such as cubes, rods, disks etc. can give us interesting perspectives into particle confinement and incorporation. Additionally, anodic aluminum oxide (AAO) membranes could also be used instead of PCTE membranes to template the synthesis of the heterostructures. AAO membranes have been promising for the synthesis of functional nanostructures due to their regular pore density, pore diameters and ease of synthesis in the lab[4]. These membranes are also stable at higher temperatures, which can open up possibilities for new composite materials.

A future goal for this work includes measurement of optoelectronic properties of the heterostructures formed by our physical confinement-based approach. We hypothesize that optoelectronic properties of the structures with more dispersed nanoparticles would be greater as there is more surface area of plasmonic nanoparticles in contact with the semiconductor to allow charge transfer. The simplest method to determine enhanced optical properties due to presence of plasmonic nanoparticles is to measure absorption or extinction spectra of the different heterostructure morphologies using UV-Visible Spectroscopy. This method can help us better understand the effects of tuning the spatial arrangement of nanoparticles in the composites and will ultimately aid

in the pursuit of constructing new and improved structures for a variety of optoelectronic applications.

References:

1. Asenath-Smith, E., Noble, J. M., Hovden, R., Uhl, A. M., DiCorato, A., Kim, Y. Y., Kulak, A. N., Meldrum, F. C., Kourkoutis, L. F. & Estroff, L. A. Physical confinement promoting formation of Cu2O-Au heterostructures with Au nanoparticles entrapped within crystalline Cu2O nanorods. *Chem. Mater.* **29**, 555–563 (2017).
2. Liu, J. H., Wang, A. Q., Chi, Y. S., Lin, H. P. & Mou, C. Y. Synergistic effect in an Au-Ag alloy nanocatalyst: CO oxidation. *J. Phys. Chem. B* **109**, 40–43 (2005).
3. Wang, C., Yin, H., Dai, S. & Sun, S. A general approach to noble metal-metal oxide dumbbell nanoparticles and their catalytic application for CO oxidation. *Chem. Mater.* **22**, 3277–3282 (2010).
4. Lee, W. & Park, S. J. Porous anodic aluminum oxide: Anodization and templated synthesis of functional nanostructures. *Chem. Rev.* **114**, 7487–7556 (2014).